(2)

ARL-TR-90-37

Copy No. 48

SPATIAL AND TEMPORAL PROPERTIES OF THE NOISE FIELD OBSERVED IN TAGEX 87

Technical Report under Contract N00024-86-C-6134, Task 1, Project 10, and Contract N00039-88-C-0043, TD Nos. 01A002 and 01A003

Clark S. Penrod
David E. Grant

APPLIED RESEARCH LABORATORIES
THE UNIVERSITY OF TEXAS AT AUSTIN
POST OFFICE BOX 8029, AUSTIN, TEXAS 78713-8029

1 November 1990

Technical Report

Prepared for:

SPACE AND NAVAL WARFARE SYSTEMS COMMAND
DEPARTMENT OF THE NAVY
WASHINGTON, DC 20363-5100

REPORT DOCUMENTATION PAGE

Form Approved
OMB No. 0704-0188

1. AGENCY USE ONLY (Leave blank)	2. REPORT DATE	3. REPORT TYPE AND DATES COVERED
	1 Nov 90	technical

4. TITLE AND SUBTITLE
Spatial and Temporal Properties of the Noise Field Observed in TAGEX 87, Technical Report under Contract N00024-86-C-6134, Task 1, Project 10 and under Contract N00039-88-C-0043, TD Nos. 01A002 and 01A003

5. FUNDING NUMBERS
N00024-86-C-6134,
Task 1, Project 10,
N00039-88-C-0043
TD Nos. 01A002, 01A003

6. AUTHOR(S)
Penrod, Clark S. Grant, David E.

7. PERFORMING ORGANIZATION NAMES(S) AND ADDRESS(ES)
Applied Research Laboratories
The University of Texas at Austin
P.O. Box 8029
Austin, Texas 78713-8029

8. PERFORMING ORGANIZATION REPORT NUMBER
ARL-TR-90-37

9. SPONSORING/MONITORING AGENCY NAME(S) AND ADDRESS(ES)
Space and Naval Warfare Systems Command
Department of the Navy
Washington, D.C. 20363-5100

10. SPONSORING/MONITORING AGENCY REPORT NUMBER

11. SUPPLEMENTARY NOTES

12a. DISTRIBUTION/AVAILABILITY STATEMENT
Approved for public release; distribution is unlimited.

12b. DISTRIBUTION CODE

13. ABSTRACT (Maximum 200 words)
This report presents an analysis of the vertical spatial structure of the near-bottom ambient noise field at a western Atlantic site, based on recorded data from a 24-element vertical line array. The properties of the noise field are discussed in terms of dominant sources and propagation mechanisms. Particular emphasis is placed on the effects of local and distant shipping on beam noise levels for a vertical array.

14. SUBJECT TERMS
ambient noise noise field directionality vertical arrays

15. NUMBER OF PAGES
65

16. PRICE CODE

17. SECURITY CLASSIFICATION OF REPORT	18. SECURITY CLASSIFICATION OF THIS PAGE	19. SECURITY CLASSIFICATION OF ABSTRACT	20. LIMITATION OF ABSTRACT
UNCLASSIFIED	UNCLASSIFIED	UNCLASSIFIED	SAR

TABLE OF CONTENTS

	Page
LIST OF FIGURES	v
LIST OF TABLES	vii
1. BACKGROUND	1
1.1 PREVIOUS WORK	1
1.2 TAGEX 87 OBJECTIVES	2
2. TAGEX 87 DATA SET AND ANALYSIS PROCEDURES	5
2.1 SITE CHARACTERISTICS	5
2.2 DATA ANALYSIS	16
2.2.1 Spectral Analysis and Beamforming	16
2.2.2 Directionality Estimation	18
3. MEASUREMENT RESULTS	21
3.1 VERTICAL DIRECTIONALITY OF THE NOISE FIELD	21
3.1.1 Sidelobe Contamination Effects	21
3.1.2 Beam Noise Measurements	23
3.2 BEAM NOISE TIMESERIES AT SELECTED ANGLES	24
3.2.1 High Angle Beams	35
3.2.2 Low Angle Beams	35
3.2.3 Broadside Beam	36
3.2.4 Vertical Dipole	36
3.3 SUMMARY OF BEAM NOISE OBSERVATIONS	36
3.3.1 Discrete Ships	38
3.3.2 Intermediate Range Shipping	41
3.3.3 Summary of Shipping Observations	42
4. MODEL CALCULATIONS	43
4.1 ANDES CALCULATIONS	43
4.2 RAY TRACE CALCULATIONS BASED ON OBSERVATIONS OF LOCAL SHIPPING	45
4.3 BEAM TRANSMISSION LOSS CALCULATIONS	46
4.4 RANGE DEPENDENCE OF BEAM NOISE CONTRIBUTIONS	52
5. SUMMARY	55
REFERENCES	57

LIST OF FIGURES

Figure		Page
2.1	TAGEX 87 Site Location	7
2.2	TAGEX 87 Sound Velocity Profile	9
2.3	Bottom Loss Measurements from the Outer Ridge of the Blake Plateau	10
2.4	ASTRAL Transmission Loss Contours for the TAGEX 87 Site	11
2.5	HITS Shipping Density Contours for the TAGEX 87 Area	13
2.6	Expected Number of Ships within a Given Range for Shipping Densities of One and Two Ships/deg^2	15
2.7	TAGEX 87 Vertical Array Configuration	17
2.8	Beam Patterns for the TAGEX 87 24-Element Vertical Array	20
3.1	Comparison of Endfire Beam Level with Reduced Omnidirectional Level at 55 Hz	22
3.2	Vertical Directionality of the TAGEX 87 Noise Field at 55 Hz	25
3.3	Beam Noise Percentile Levels at 55 Hz from TAGEX 87	27
3.4	Beam Noise Timeseries at 55 Hz	28
3.5	Vertical Dipole Beam and Average Omnidirectional Element Timeseries at 55 Hz	37
3.6	Beam Noise Timeseries at 55 Hz Surrounding a Merchant Ship Passage	39
4.1	Comparison of ANDES Predictions with Measured Beam Noise	44
4.2	Modeled Time Dependence of Vertical Directionality	47
4.3	Ray Trace Calculations of Transmission Loss at 50 Hz	49
4.4	ANDES Calculation of Beam Noise Levels versus Radius of Exclusion	53

LIST OF TABLES

Table		Page
2.1	Summary of Noise Spectrum Levels at Selected Frequencies.....	16
3.1	Beam and Omnidirectional Noise Levels During Four Time Periods	41

1. BACKGROUND

This report describes measurements of vertical directionality of the low frequency ambient noise field near the ocean bottom at a North Atlantic site approximately 300 nmi east of Jacksonville, Florida. The site was near the outer ridge of the Blake Plateau at 4570 m depth. In addition to obtaining directionality measurements at this particular site, the objective of the experiment was to improve understanding of the environmental mechanisms which determine spatial properties of the noise field near the ocean bottom.

1.1 PREVIOUS WORK

Previous work involving spatial properties of the ambient noise field can be traced to Anderson,[1] who was an early proponent of the need to study both temporal fluctuations and directionality properties. Anderson's early work involved the development of measurement techniques and arrays. In approximately the same time period, Stone[2] provided an excellent discussion of measurement techniques and pitfalls associated with directionality measurements based on linear arrays. Both of these works remain relevant in light of current interest in spatial properties of ocean ambient noise fields.

Several early papers were concerned with spatial properties of noise at frequencies from 300 Hz up to several kilohertz. Measurements in the octave from 750 Hz to 1500 Hz with a 32-element volumetric array (based on Anderson's work) at depths of 300-600 m were reported by Becken,[3] and by Rudnick and Squier.[4] This work focused primarily on noise generated by the interaction of wind and waves at the sea surface, and identified a directionality function for the radiation of this noise source. Forster[5] described similar measurements in the 800-5000 Hz band from a 21-element 5 m vertical line array at the ocean bottom at a depth of 4300 m.

Among the papers dealing with ship dominated noise at lower frequencies is the work of Axelrod et al.,[6] who presented measurements from a bottomed vertical line array at a site near Bermuda. The array consisted of 40 elements in a geometrically tapered line with a total aperture of 91 m. Measurements included vertical directionality of the ambient noise field at frequencies of 100-1500 Hz. The measurements spanned a period of approximately eight months, and were edited to exclude strong nearby sources such as ships, whales, and SUS events. At 112 Hz, the measurements revealed a strong bias toward low angle arrival of noise energy, with a difference of 20 dB between vertical and horizontal arrival angles. The directionality was reversed at the higher frequencies where

the dominant arrival angles were near vertical, but the anisotropy was not as great, amounting to only 8 dB at 1414 Hz. Similar measurements were reported by Fox,[7] based on essentially the same array. A comparison of these two papers reveals some interesting similarities and differences. Both papers reported similar levels for the low angle energy at 200 Hz. However, Fox's results indicate much higher levels at the steeper angles for a given sea state. For example, at SS5, Fox reported approximately 64 dB//μPa^2/steradian-Hz, while Axelrod reported 54 dB at the same sea state. As a result, the directionality reported by Fox showed much less anisotropy than that reported by Axelrod.

In a more recent measurement, Anderson[8] obtained data from a vertical array suspended at various depths below FLIP (floating instrumentation platform, a manned 350 ft spar buoy operated by The University of California, San Diego, Marine Physical Laboratory). The array spanned 532 m, included 20 elements, and was used to obtain measurements of vertical directionality at frequencies between 23 and 100 Hz. These results again showed a strong anisotropy with the noise dominated by low angle arrivals.

The generally accepted interpretation of the low frequency directionality observed in these experiments is that the noise from ships at "long" ranges is in effect filtered by the angular dependence of the bottom loss. Propagation to a near-bottom sensor involves a bottom interaction on each ray cycle for all rays except those which turn above the bottom. In areas where the bottom is well sedimented, rays which interact with the bottom at shallow grazing angles are not heavily attenuated by the bottom loss. However, at steeper grazing angles, the increased bottom loss and reduced ray cycle distance result in attenuation of the energy at those angles. The net result is an anisotropy favoring lower angles when the noise field is dominated by distant source conditions.

1.2 TAGEX 87 OBJECTIVES

The TAGEX 87 experiment was prompted by recent interest in the relationships between noise source distribution and the spatial properties of the near-bottom ambient noise field. The experiment was designed to obtain a high resolution measurement of the vertical structure of the near-bottom noise field in the deep ocean basin between Bermuda and the U.S. coast.

A major objective of the analysis reported here is to extend understanding of the noise environment through an analysis of the impact of shipping distributions on the characteristics of the noise field. The basic nature of the spatial and temporal properties of

the noise field depends on the number of sources which are significant contributors. Intuitively, one would expect that if the low frequency noise field is dominated by the superposition of contributions from a large number of ships distributed over a large ocean area, then it should be a relatively stable process. Aside from the effects of seasonal changes, large scale weather patterns, and the occasional ship passing within direct path range, fluctuations in level should be minor. On the other hand, if the low frequency noise field is dominated by a relatively small number of ships within 50-100 miles of the array, then we may expect the noise process to be less stable. The TAGEX 87 data set offers an opportunity to examine these hypotheses as they relate to noise in various vertical angular sectors.

In the following sections, we will examine the characteristics of the ocean environment in the exercise area, and then present an analysis of measurements made with a 230 m vertical line array.

2. TAGEX 87 DATA SET AND ANALYSIS PROCEDURES

2.1 SITE CHARACTERISTICS

The TAGEX 87 experiment was conducted in the western Atlantic at approximately 29°N, 74°W, as shown in Fig. 2.1. The site is about 300 nmi from the East Coast, 150 nmi from the edge of the continental shelf; water depth at the site is approximately 4570 m. The site is west of the Hatteras Abyssal Plain, near the Outer Ridge of the Blake Plateau.

A sound velocity profile, shown in Fig. 2.2, indicates that the bottom is slightly below critical depth for a shallow source. Direct path propagation to a near-bottom sensor occurs to ranges of about 18 nmi. This portion of the basin is considered to have a thickly sedimented, low loss bottom. Bottom loss measurements taken from NADC data[9] at octave spacings between 50 and 1600 Hz are shown in Fig. 2.3. These measurements, fairly typical of a thickly sedimented Atlantic basin, indicate that for bottom grazing angles less than 20°, there is very low loss at 50 Hz. Above 20°, the loss increases substantially to 10-20 dB per bounce for grazing angles above 35°.

ASTRAL transmission loss contours for the site are shown in Fig. 2.4. These calculations are for a shallow source at 50 Hz. The 80 dB contour is slightly within the direct path range at about 12 nmi. The 90 dB contour lies at about 25 nmi, with the 100 dB contour falling at approximately 75 nmi. Each of these first three contours is roughly circular; however, the 110 dB contour is affected by the continental shelf and the Blake Plateau to the west of the site. Looking to the west, 110 dB loss occurs at about 150 nmi, while to the east it occurs at 200 nmi.

The HITS shipping database for the region is contoured in Fig. 2.5. Contoured densities are at 0.5, 1.0, 2.0, and 4.0 ships/deg^2. The contours show a major coastal shipping lane with densities of 2 to 4+ ships/deg^2, and a trans-Atlantic lane carrying traffic from the Gulf of Mexico to Europe, with densities of 0.5 to 2+ ships/deg^2. However, most of the area with shipping density greater than 2 ships/deg^2 lies outside of the 110 dB transmission loss contour. Within 100 nmi of the site, the shipping density is between 1 and 2 ships/deg^2.

Figure 2.6 shows the mean number of ships expected to lie within a given radius of the site for shipping densities of 1 and 2 ships/deg^2. The figure indicates that

BATHYMETRY CONTOURS

RED = 0 m
BROWN = 1000 m
GREEN = 2000 m
CYAN = 3000 m
BLUE = 4000 m
VIOLET = 5000 m

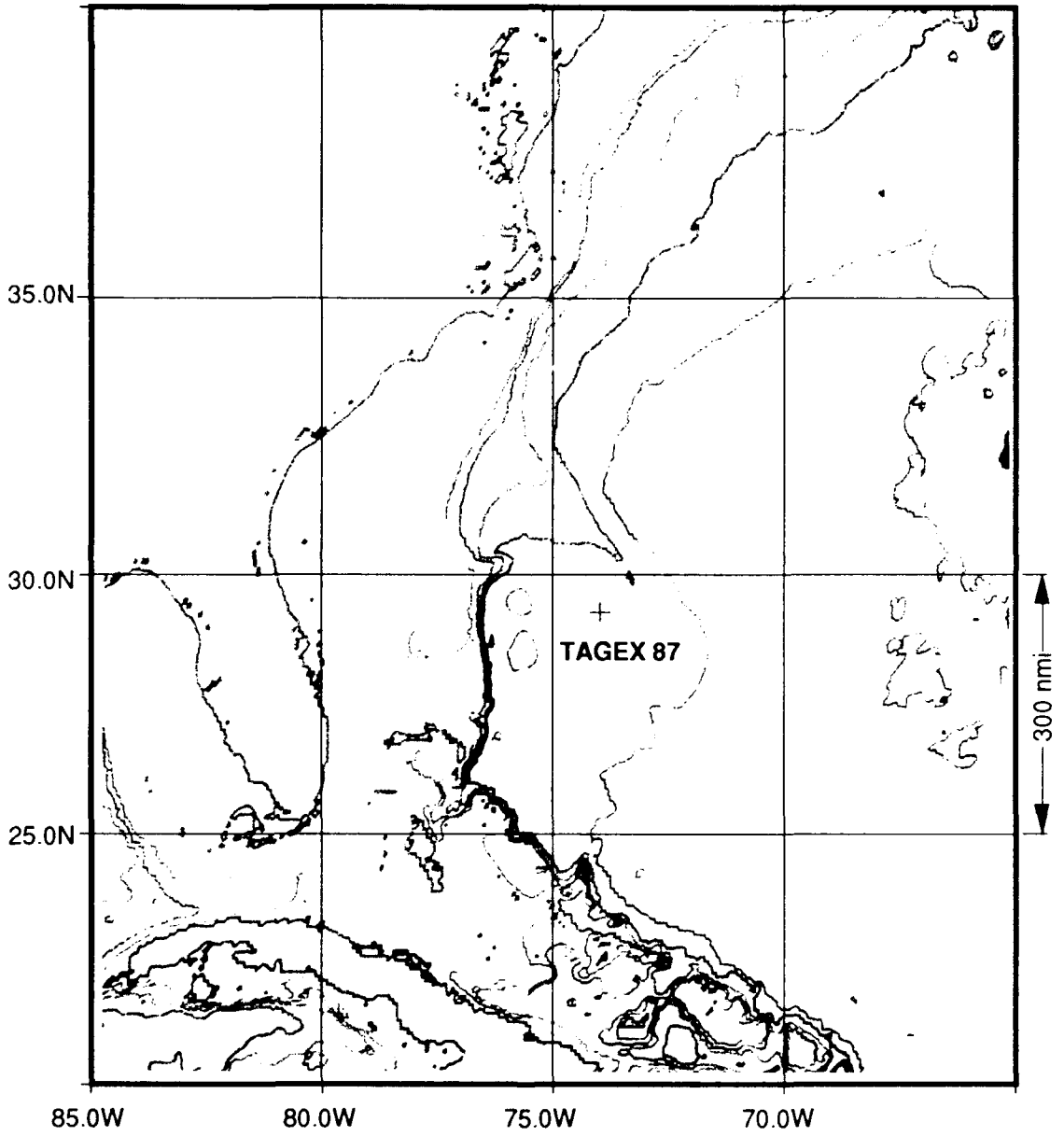

FIGURE 2.1
TAGEX 87 SITE LOCATION

ARL:UT
AS-90-916
CSP - DS
12 - 17 - 90

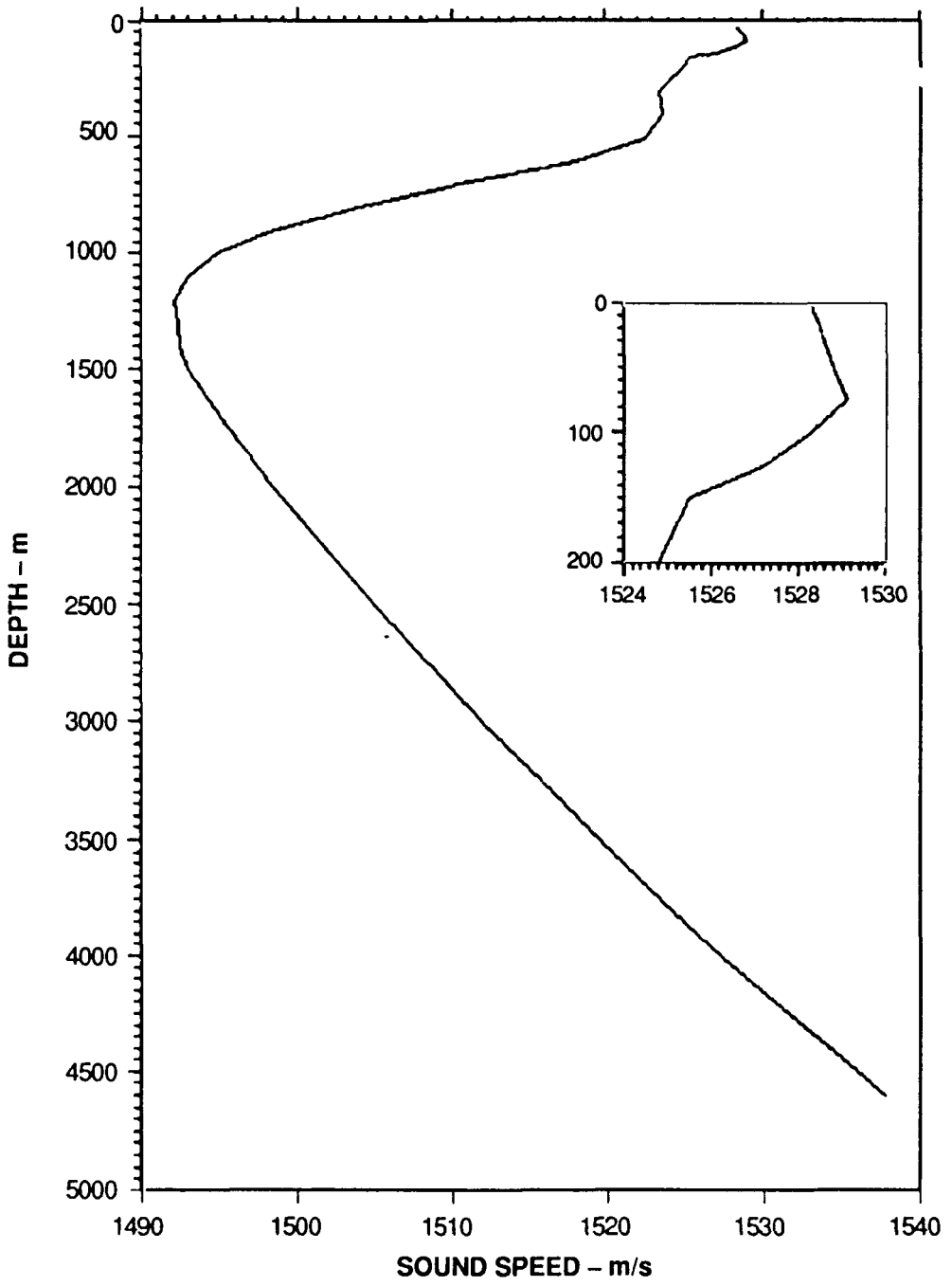

FIGURE 2.2
TAGEX 87 SOUND VELOCITY PROFILE

ARL:UT
AS-90-917
CSP - DS
12 - 17 - 90

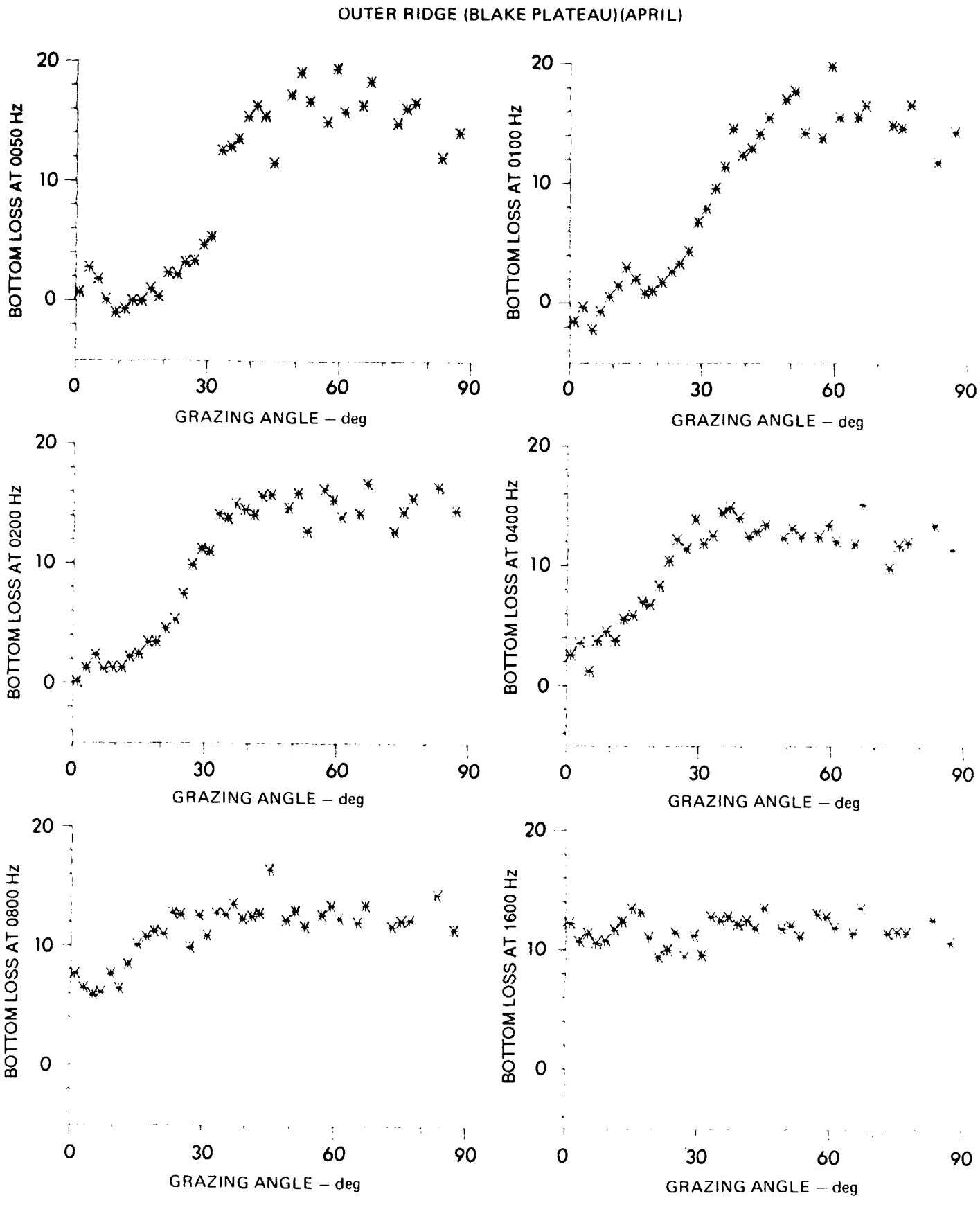

FIGURE 2.3
BOTTOM LOSS MEASUREMENTS FROM THE OUTER RIDGE OF THE BLAKE PLATEAU

ARL UT
AS-80-1373
JFL - GA
7 - 24 - 80

TRANSMISSION LOSS
20 ft TARGET DEPTH
MAY, 50 Hz

RED = 80 dB
BROWN = 90 dB
GREEN = 100 dB
BLUE = 110 dB

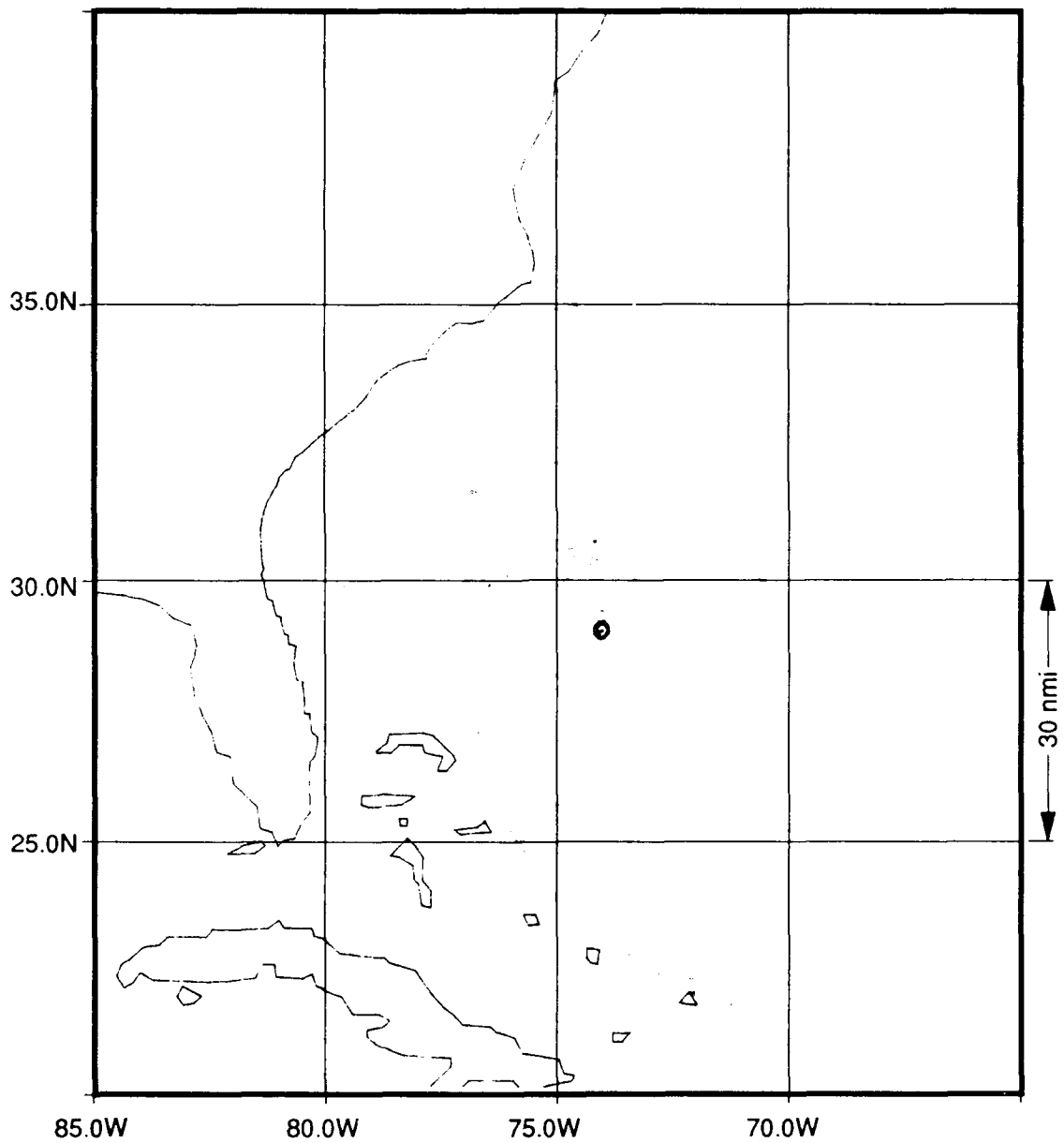

FIGURE 2.4
ASTRAL TRANSMISSION LOSS CONTOURS
FOR THE TAGEX 87 SITE
SOURCE DEPTH = 6 m

ARL:UT
AS-90-919
CSP - DS
12 - 17 - 90

RED = 0.5 SHIPS/deg^2
BROWN = 1.0 SHIPS/deg^2
GREEN = 2.0 SHIPS/deg^2
CYAN = 4.0 SHIPS/deg^2

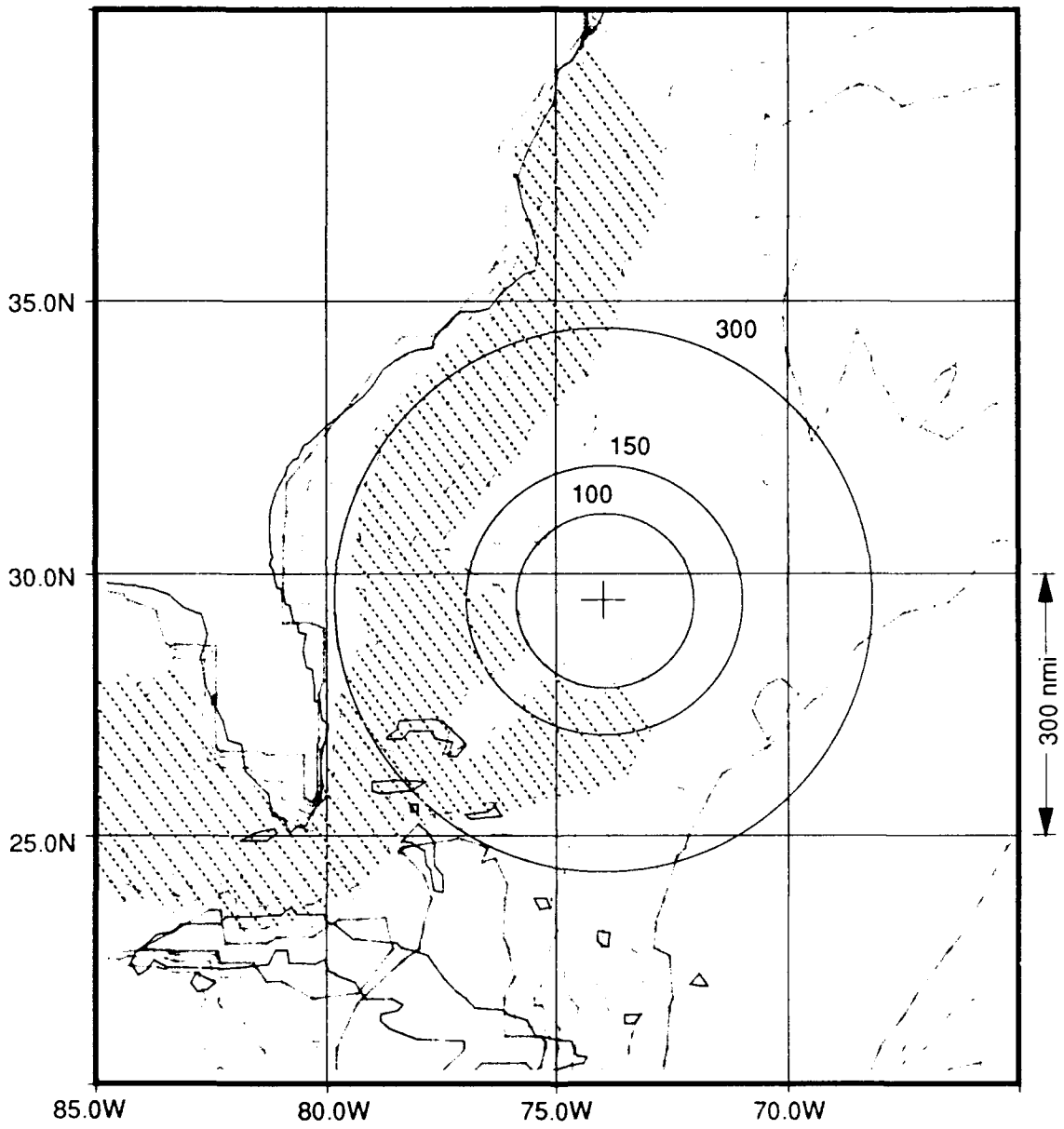

FIGURE 2.5
HITS SHIPPING DENSITY CONTOURS FOR THE TAGEX 87 AREA

ARL:UT
AS-90-920
CSP - DS
12 - 17 - 90

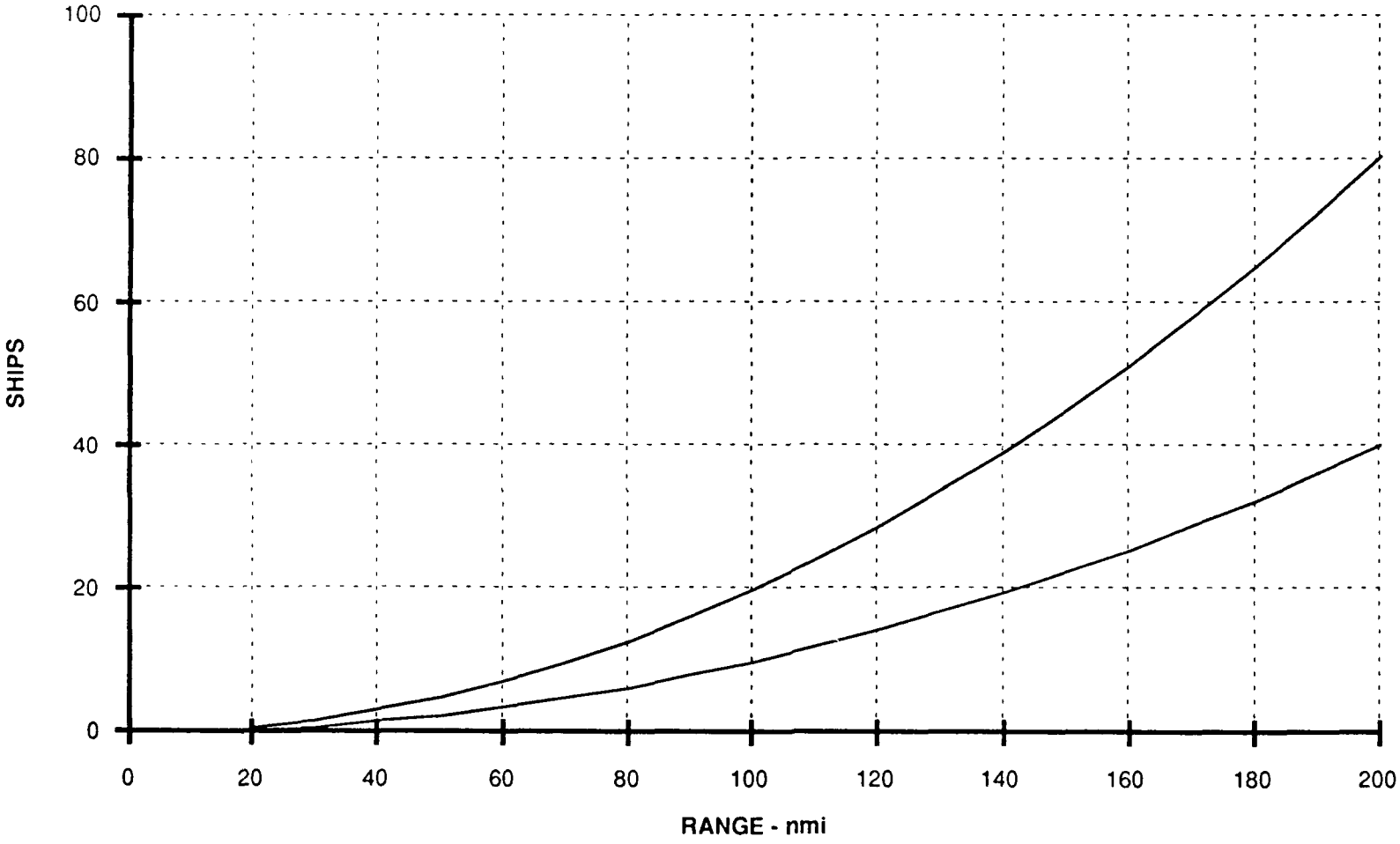

FIGURE 2.6
EXPECTED NUMBER OF SHIPS WITHIN A GIVEN RANGE FOR SHIPPING DENSITIES OF ONE AND TWO SHIPS/deg^2

10-20 ships are expected to be within a range of 100 nmi of the site at any given time. Of course, the actual number of ships present at any given time is a random variable.

Omnidirectional noise statistics for the bottom element of the array from this experiment are summarized in Table 2.1. The low frequency levels are consistent with moderate shipping densities, while the levels at 300 Hz are consistent with the 10-15 kt median wind speeds observed during the exercise.

TABLE 2.1

SUMMARY OF NOISE SPECTRUM LEVELS AT SELECTED FREQUENCIES

Frequency (Hz)	90th (dB)	50th (dB)	10th (dB)	σ (dB)
25	85.5	82.5	80.6	2.5
50	88.2	83.1	79.6	4.0
150	73.9	69.9	67.5	2.8
300	67.0	63.3	59.8	2.9

2.2 DATA ANALYSIS

2.2.1 Spectral Analysis and Beamforming

In addition to various other sensors deployed within a few miles of the site, the array shown in Fig. 2.7 was deployed and recorded with a VEDABS system. The array was configured as a 25-element array with uniform 10 m spacing, giving a design frequency of 75 Hz. In addition to these 25 hydrophones, a hydrophone was positioned 6.1 m from the bottom of the array. Four different subsets of the array elements were used for measurements: (1) the subset consisting of hydrophones 3-26, a 24-element array, was used for vertical noise directionality, (2) and (3) the subset consisting of hydrophones 11-26, a 16-element array, and the subset consisting of hydrophones 7-18, an 8-element array, were used for vertical array beam noise and noise gain measurements, and (4) a subset consisting of hydrophones 4 and 5 was used for dipole beam noise measurements. Noise field directionality and beam noise measurements were made at 63 Hz and 55 Hz. Differences observed between these two frequencies were minor; only

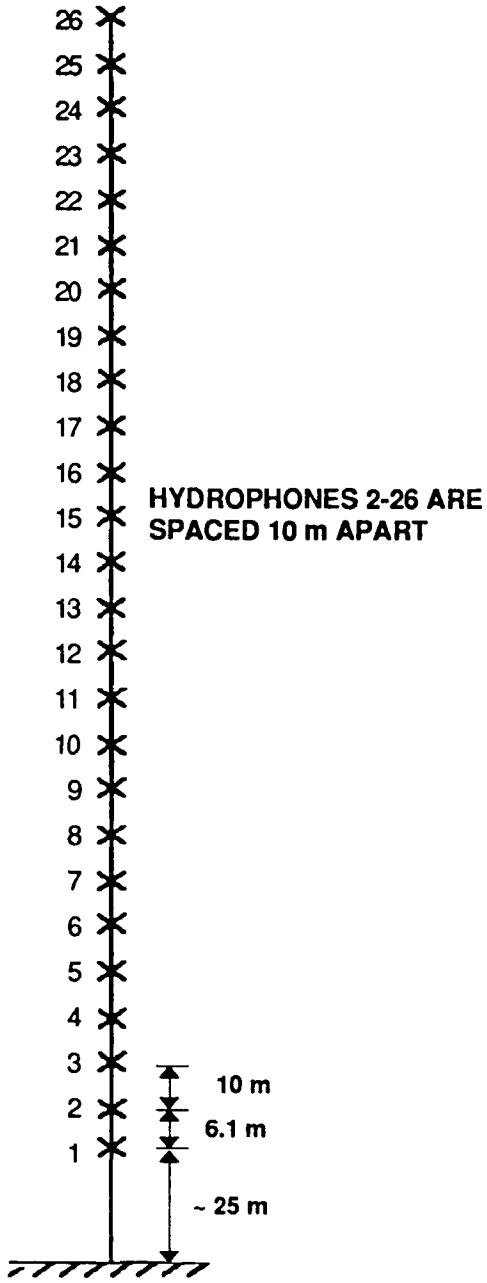

FIGURE 2.7
TAGEX 87 VERTICAL ARRAY CONFIGURATION

the 55 Hz data based on the 24-element array are presented here. Measurements of vertical dipole beam noise at 55 Hz will also be presented.

The data were processed by forming an estimate of the noise cross-spectral-matrix based on the average of non-overlapped FFTs. Such an estimate was formed every 10 min from approximately 1 min of digitized data. The data were digitized at 150 Hz, and 35 256-point FFTs were used in each cross-spectral-matrix estimate. The basic frequency resolution of the cross-spectra was 0.59 Hz, but because the Hanning window was used, the effective spectral resolution of the data was 0.88 Hz.

2.2.2 Directionality Estimation

A primary motivation for the experiment was to obtain an estimate of the directionality properties of the noise field, based on data from the vertical line array described in the preceding section. An estimate of the vertical directionality of the noise field can be obtained by steering beams from endfire to endfire and measuring the angular dependence of the beam noise. However, as Stone points out, such an estimate can be corrupted by various factors. For example, if the beam noise is not dominated by energy arriving within the main lobe, but rather is influenced by sidelobe contributions, the resulting estimate will be misleading. Also, if the basic directionality of the field has features which are small compared to the beamwidth of the array, these features will be smoothed out in the estimated directionality.

Various techniques have been suggested for dealing with these problems. These include solving a set of linear equations involving beam noise measurements at selected steering angles,[10] or assuming that the noise field as represented by the cross-spectral-matrix is an analytic function and can be decomposed into plane waves.[11] In this report, we have chosen to simply present the beam noise measurements, making note of the limitations on the resulting directionality estimate which result from the array parameters. We have been more concerned with measurement of relatively gross features of the directionality than fine structure; hence, we have shaded the array to reduce sidelobes, accepting the resulting penalty in increased beamwidth.

Dolph-Chebyshev shading was used to reduce the sidelobe levels. Although shading coefficients can be derived for any desired sidelobe level, the effects of amplitude and phase errors in the calibration of the hydrophones and recording system will conspire to limit the amount of reduction in sidelobe level which can be achieved with conventional

beamforming. In the following section, we will describe procedures used to determine the extent to which sidelobe suppression was successful in reducing leakage problems.

The other factor limiting directionality measurement is the beamwidth. For the 24-element Dolph-Chebyshev shaded array used, the broadside beamwidth is approximately 7°, broadening significantly toward endfire. Beam patterns for this array at four steering angles are shown in Fig. 2.8. Since our greatest interest in the structure of the noise field lies at lower grazing angles where shipping dominates, the coarse resolution of our estimate near endfire is not a significant factor.

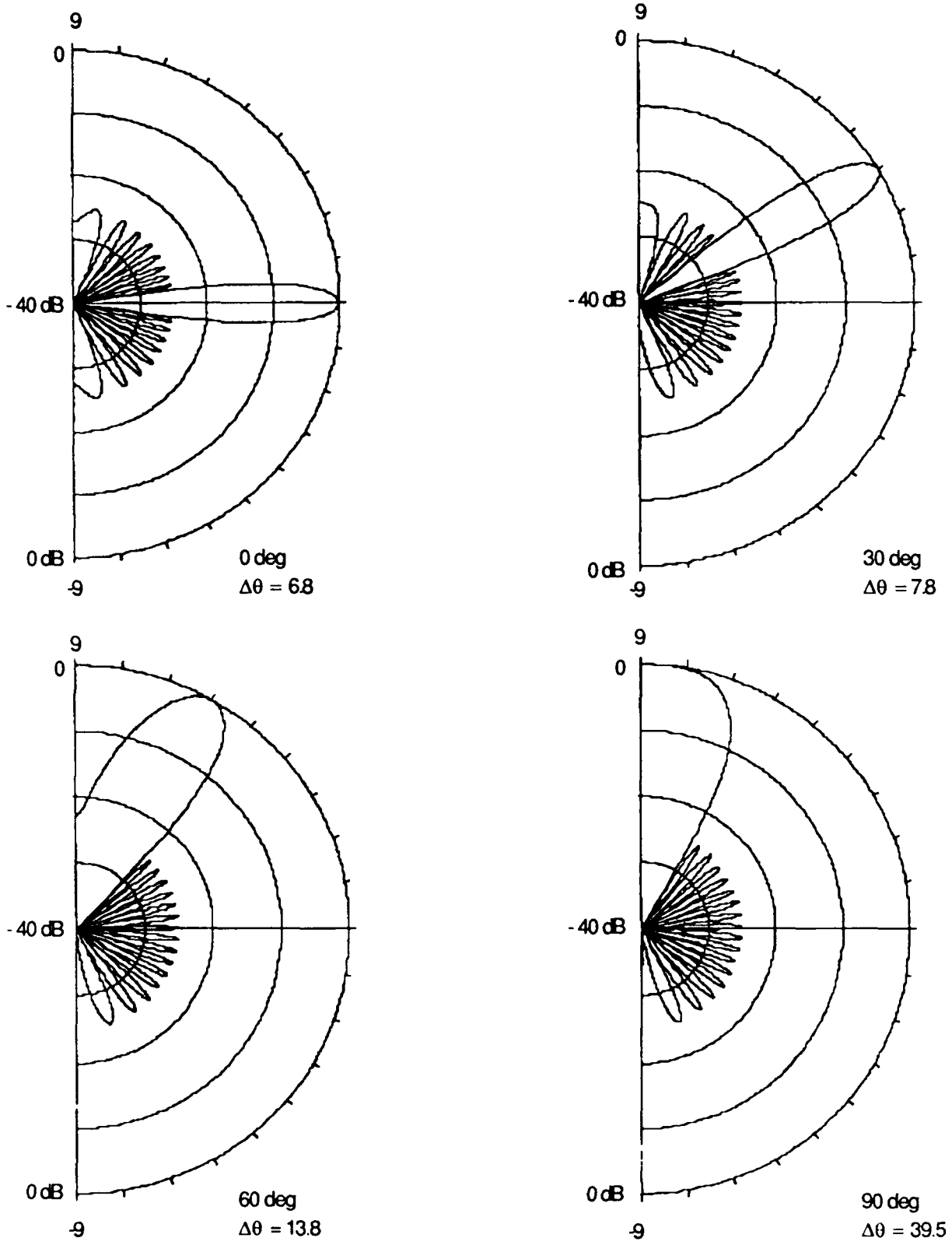

FIGURE 2.8
BEAM PATTERNS FOR THE TAGEX 87
24-ELEMENT VERTICAL ARRAY

ARL:UT
AS-90-923
CSP - DS
12 - 17 - 90

3. MEASUREMENT RESULTS

3.1 VERTICAL DIRECTIONALITY OF THE NOISE FIELD

As indicated above, one of the primary difficulties involved in analysis of this data set involves the strong anisotropy between the near-horizontal angles dominated by distant shipping and the vertical angles dominated by local wind and waves. In this section, we first describe the results of an analysis of sidelobe contamination effects; these results are needed to properly interpret the beam noise measurements presented later.

3.1.1 Sidelobe Contamination Effects

A method for identifying sidelobe leakage problems was suggested by Hanna.[12] In the absence of nearby ships, the endfire beam pointed toward the sea surface should ideally be dominated by surface generated noise due to wind and wave action. However, when the low angle component due to distant shipping is at a sufficiently high level relative to the surface generated noise, it may dominate the endfire beam noise through sidelobe leakage. Sidelobe contributions to the endfire beam noise can be estimated by reducing the low angle noise level by an amount corresponding to the average sidelobe level. Provided that we know what the average sidelobe level is, we can test for sidelobe contamination by comparing the endfire beam noise with the distant shipping noise (or, equivalently, the omnidirectional noise) reduced by the average sidelobe level.

To estimate the sidelobe suppression achievable with this array, endfire beam levels were measured with shading for various sidelobe levels. The results showed that endfire beam levels were reduced as additional sidelobe suppression was added until the sidelobes were at approximately -25 dB. At that point, further reduction in sidelobe level had little effect on the endfire beam noise level. This suggests that either the array does not support sidelobe suppression below -25 dB, or that the endfire beam noise is not sidelobe contaminated when sidelobes are below -25 dB.

In Fig. 3.1, we show timeseries of the omnidirectional level reduced by 25 dB, compared with the endfire beam level at 55 Hz for the entire data set. The reduced omnidirectional level lies consistently within 2 dB of the endfire beam level and appears to be strongly correlated, indicating that the endfire beam noise is undoubtedly dominated by sidelobe contributions from the low angle energy. This is not surprising since we would expect wind generated noise levels of 60-65 dB for the wind conditions existing during the

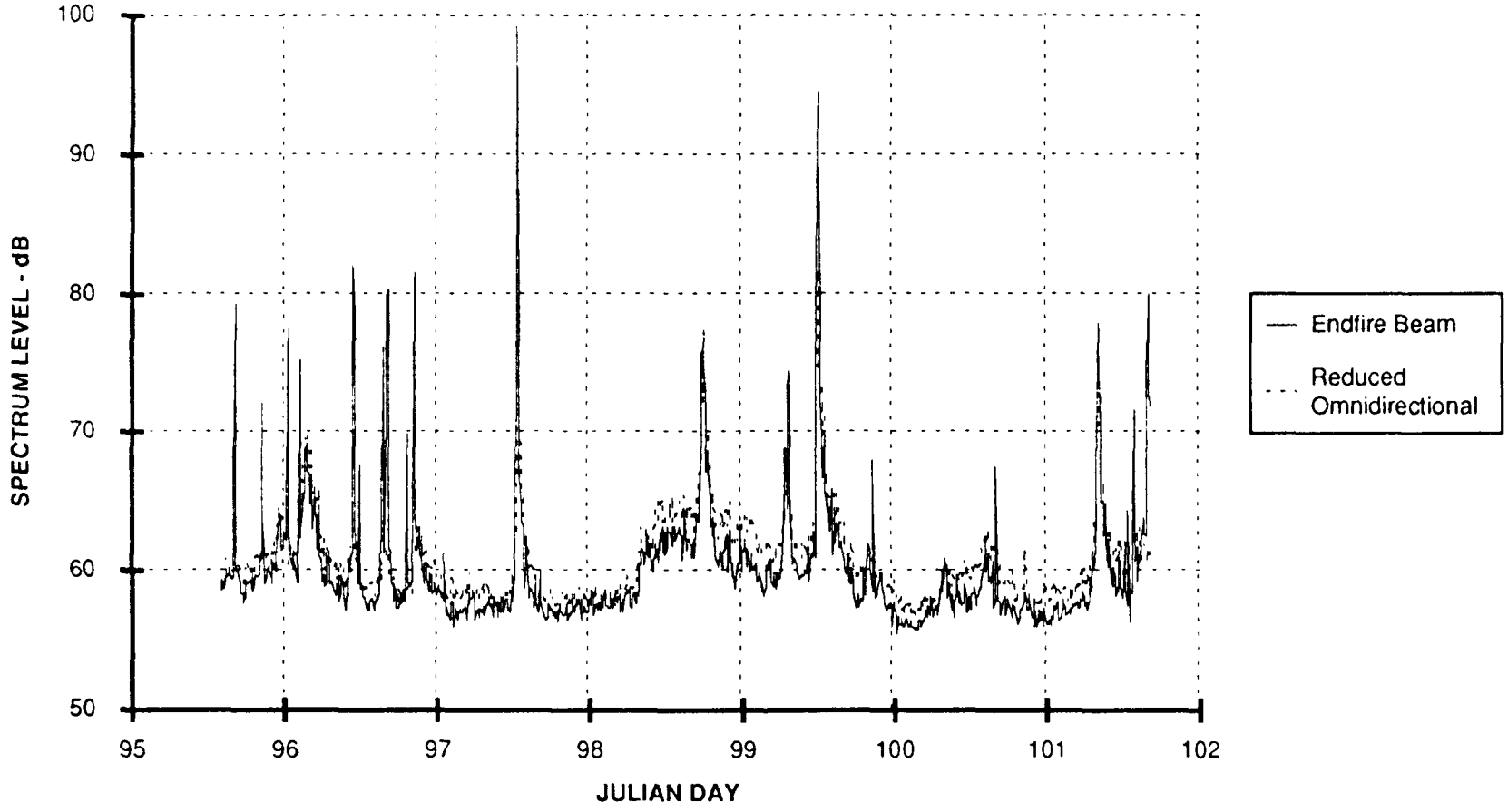

FIGURE 3.1
COMPARISON OF ENDFIRE BEAM LEVEL WITH REDUCED OMNIDIRECTIONAL LEVEL AT 55 Hz

ARL:UT
AS-90-924
CSP - DS
12 - 17 - 90

exercise. The directivity index of the endfire beam for this array is approximately 12.5 dB at this frequency, indicating that we should expect beam noise levels of approximately 50 dB due to local winds. In order to measure these low levels, sidelobe suppression of nominally 40 dB would be required. Since such sidelobe suppression is apparently not achievable with this array, we should regard the beam noise measurements for the higher angle beams as an upper bound.

3.1.2 Beam Noise Measurements

Beam noise measurements were made for steering angles from endfire to endfire in 1° increments. To obtain a broad perspective of the directionality properties and variability of the noise field, the results are presented in Fig. 3.2 in a color coded format in units of dB//μPa^2/Hz. (Note that these measurements represent beam noise, and are not normalized to account for beamwidth.) The angle axis is oriented so that positive angles are toward the surface and negative angles toward the bottom. The time axis is in a Julian day/hour/minute format, and spans a period of approximately six days.

The most obvious feature in Fig. 3.2 is the broad swath of energy at arrival angles between ±30°. This is the component generally attributed to distant shipping. The quiet levels at steeper angles are occasionally interrupted by the passage of nearby ships. Multipath structure associated with these individual ships can sometimes be seen, as is the case with the events at 98/18 and 99/12. Note that these events exhibit aspect dependence of surface ship source levels in that additional multipaths are visible for a longer period when the ship is going away from the array.

Figure 3.3 displays the same data in a percentile format, where percentile levels are obtained for each 2° angular bin. From this display, one can see that median beam noise levels of 78 dB occur near 0°, whereas the median beam level at 45° is roughly 60 dB. The difference is a measure of the anisotropy in the noise field, although we must bear in mind that the levels measured at the steeper angles are contaminated with leakage from the low angle noise. Hence the actual anisotropy is greater than indicated in Fig. 3.3.

The data in Fig. 3.3 also reveal the angular regions where the greatest variability occurs due to local and intermediate range shipping. In the sector between ±5°, the 10^{th} and 90^{th} percentiles are separated by only 4 dB. However, between 10° and 30°, the spread between these two percentiles steadily increases to a value of 16 dB at 30°. The spread then decreases above 30° to a value of 8 dB at 50°; however, note that much of the

variability above 50° is due to leakage of low angle energy through the sidelobes of the beam pattern. Hence, the variability at steep angles is probably much less than indicated, as would be expected from the benign weather conditions during the measurements.

The percentile displays suggest that the vertical directionality of the noise field can be described in terms of three angular sectors. The low angles within 10° of horizontal are fairly stable and tend to be dominated by distant shipping noise propagating in low loss paths which graze the bottom at very low angles. Between 10° and 40° on either side of horizontal, we see a much less stable process apparently driven by the effects of local and intermediate range shipping. At steeper angles above 40°, we expect to see a relatively stable process which is dominated by weather effects. This interpretation is consistent with the generally accepted version which has appeared in the literature for many years, with the significant difference that the shipping noise at angles below 40° can be separated into two distinct components: the first due to truly long range shipping at very low angles (≤10°), and the second, a more dynamic component due to a smaller number of ships at intermediate ranges. The following section on beam noise timeseries will further illustrate these distinct components.

3.2 BEAM NOISE TIMESERIES AT SELECTED ANGLES

In this section we present timeseries displays of beam noise from the 24-element array. Figures 3.4(a)-(g) show beam noise for steering angles of 0° (broadside), 10°, 20°, 30°, 45°, 60°, and 90° (endfire toward surface). Each plot also contains the average omnidirectional timeseries for reference. The omnidirectional sensor and the beams steered off broadside reveal several events of relatively short duration during which the levels rise rapidly for a period of a few hours. As pointed out above, these are caused by nearby passages of ships, several of which were tracked by the radar aboard USNS ZEUS (T-ARC 7), which maintained station approximately 12 nmi from the VEDABS site throughout the recording period. All but one of the CPA events prior to day 97 were due to USNS NEPTUNE (T-ARC 2), towing a projector. The single event not due to USNS NEPTUNE occurred in the early hours of day 96, and is of somewhat longer duration than the USNS NEPTUNE events. On day 98, USNS NEPTUNE left the area.

In the following discussion, the beam noise timeseries are divided into three groups which share similar characteristics. Each group is discussed separately.

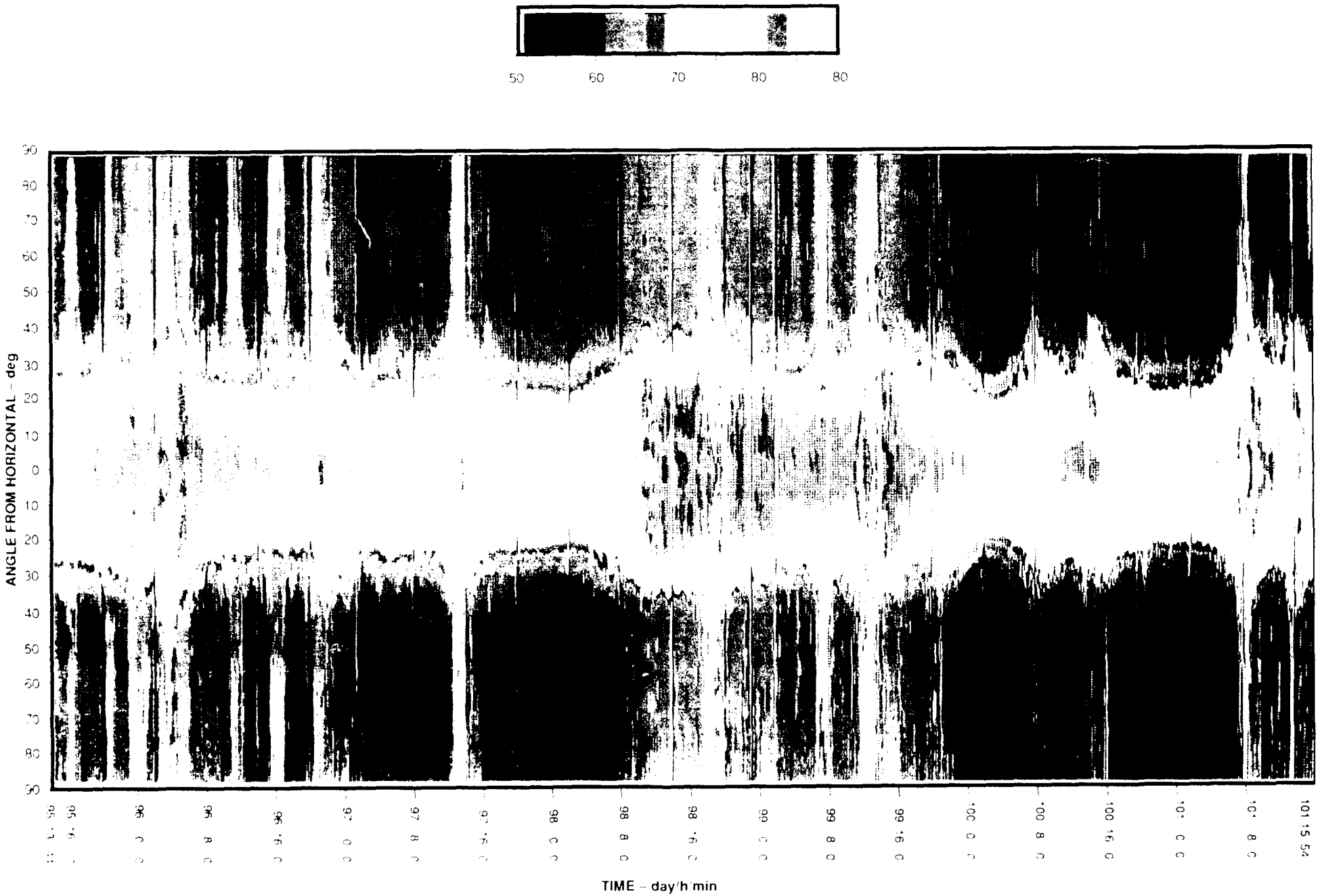

FIGURE 3.2
VERTICAL DIRECTIONALITY OF THE TAGEX 87 NOISE FIELD AT 55 Hz

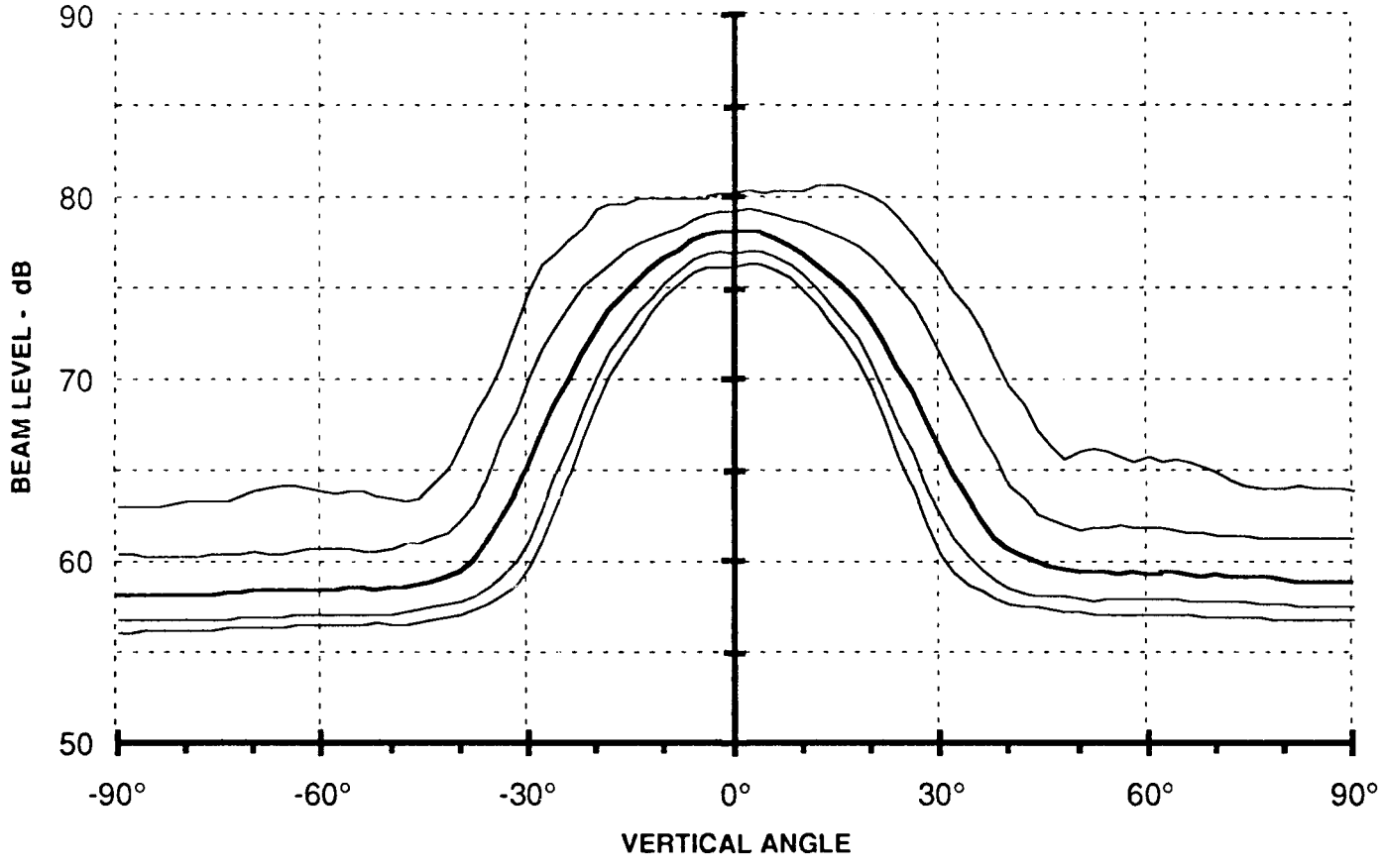

FIGURE 3.3
BEAM NOISE PERCENTILE LEVELS AT 55 Hz FROM TAGEX 87
(10th, 25th, 50th, 75th, 90th PERCENTILES)

ARL:UT
AS-90-926
CSP-DS
12-17-90

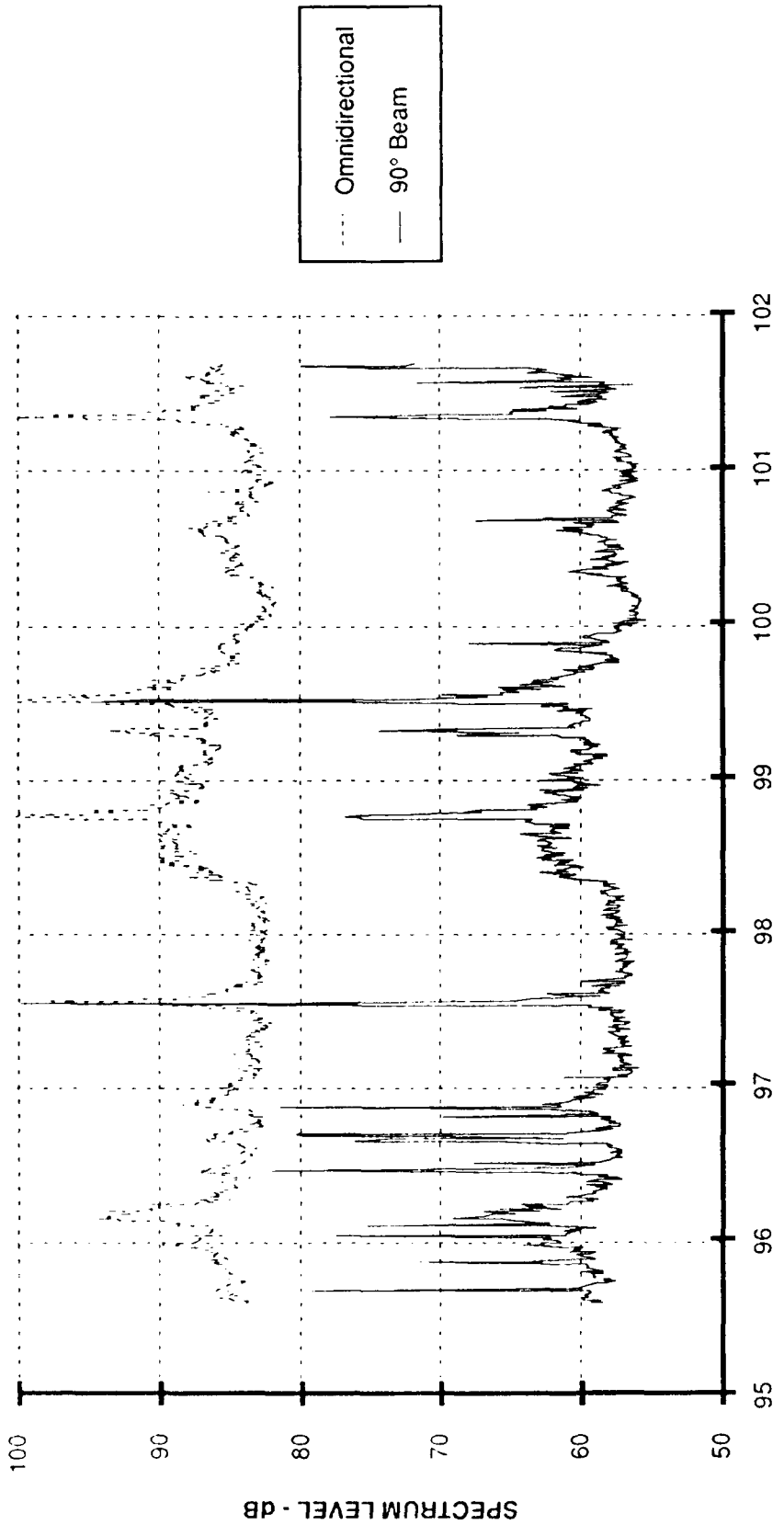

(a) 90° Beam

FIGURE 3.4
BEAM NOISE TIMESERIES AT 55 Hz

ARL:UT
AS-90-927
CSP - DS
12 - 17 - 90

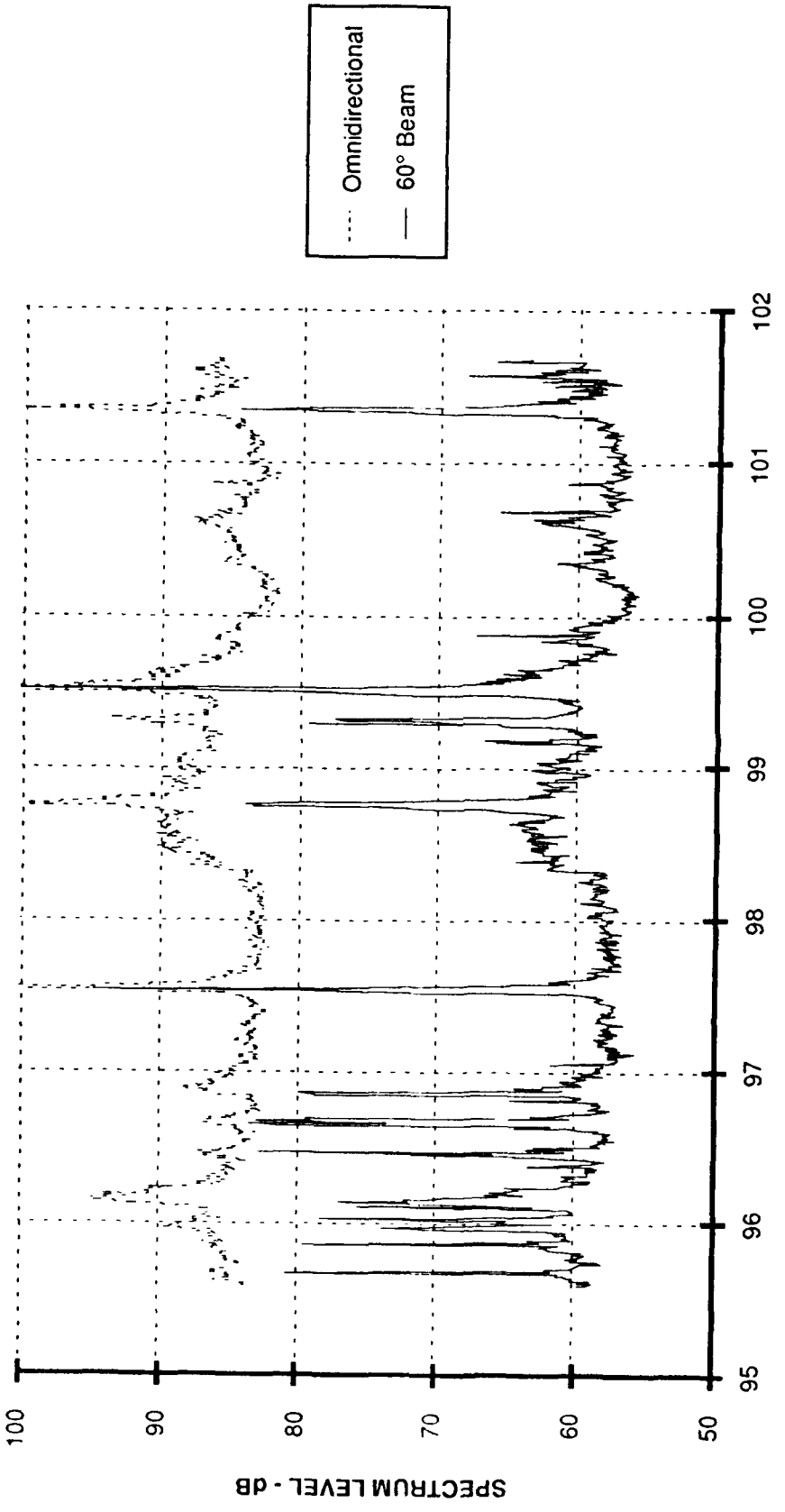

(b) 60° Beam

FIGURE 3.4 (cont'd)
BEAM NOISE TIMESERIES AT 55 Hz

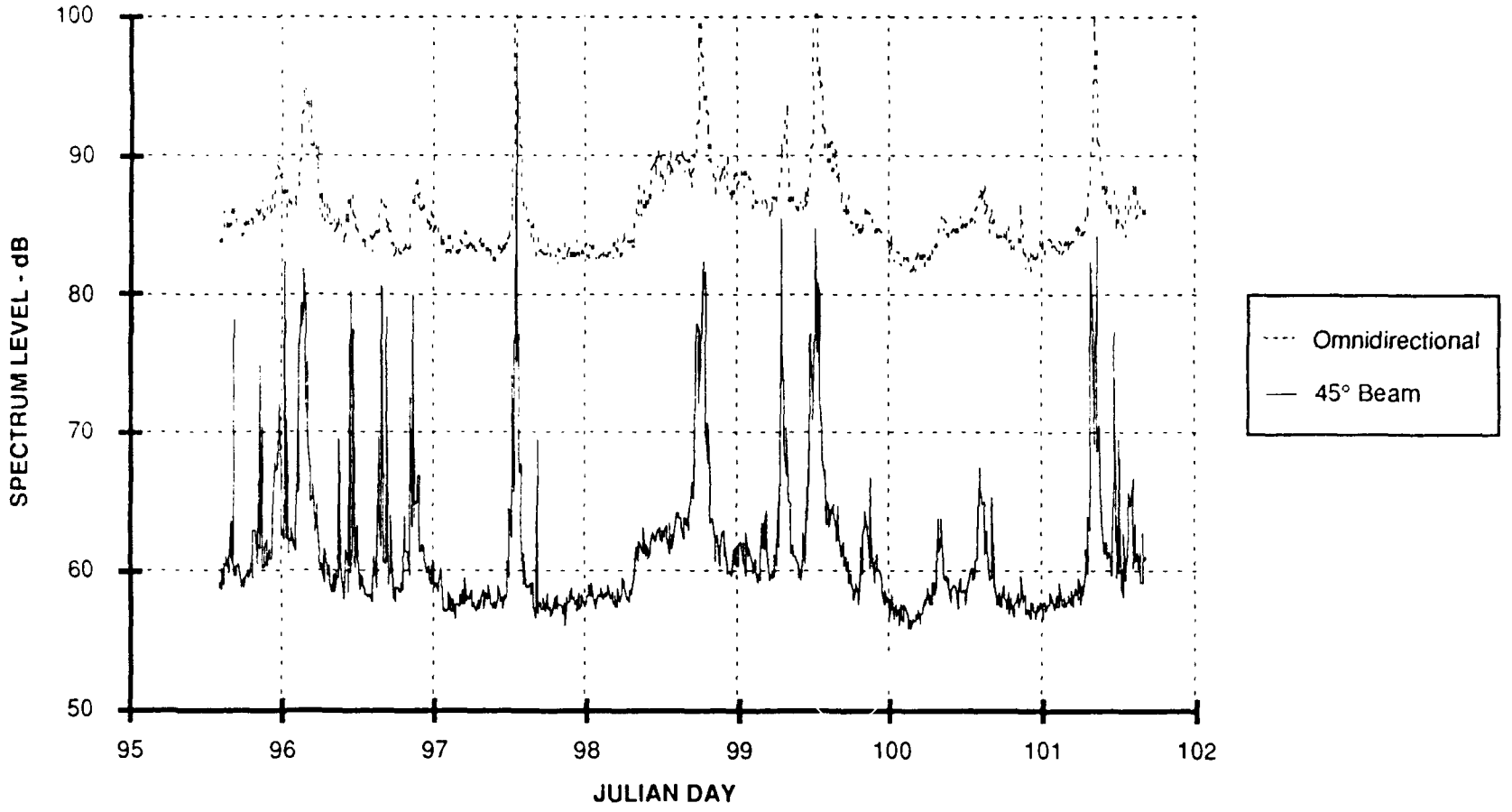

(c) 45° Beam

FIGURE 3.4 (cont'd)
BEAM NOISE TIMESERIES AT 55 Hz

ARL:UT
AS-90-929
CSP - DS
12 - 17 - 90

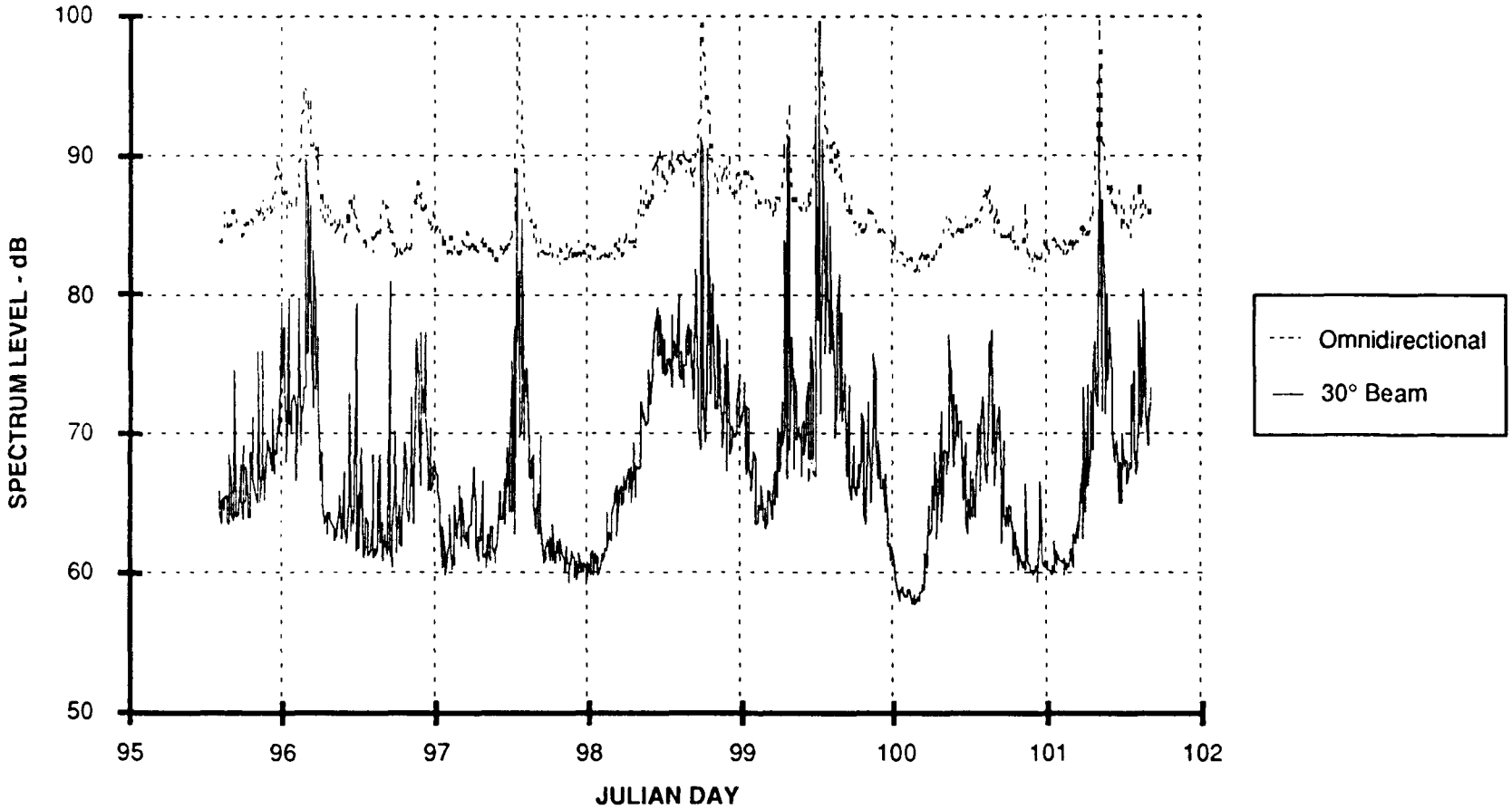

(d) 30° Beam

FIGURE 3.4 (cont'd)
BEAM NOISE TIMESERIES AT 55 Hz

ARL:UT
AS-90-930
CSP - DS
12 - 17 - 90

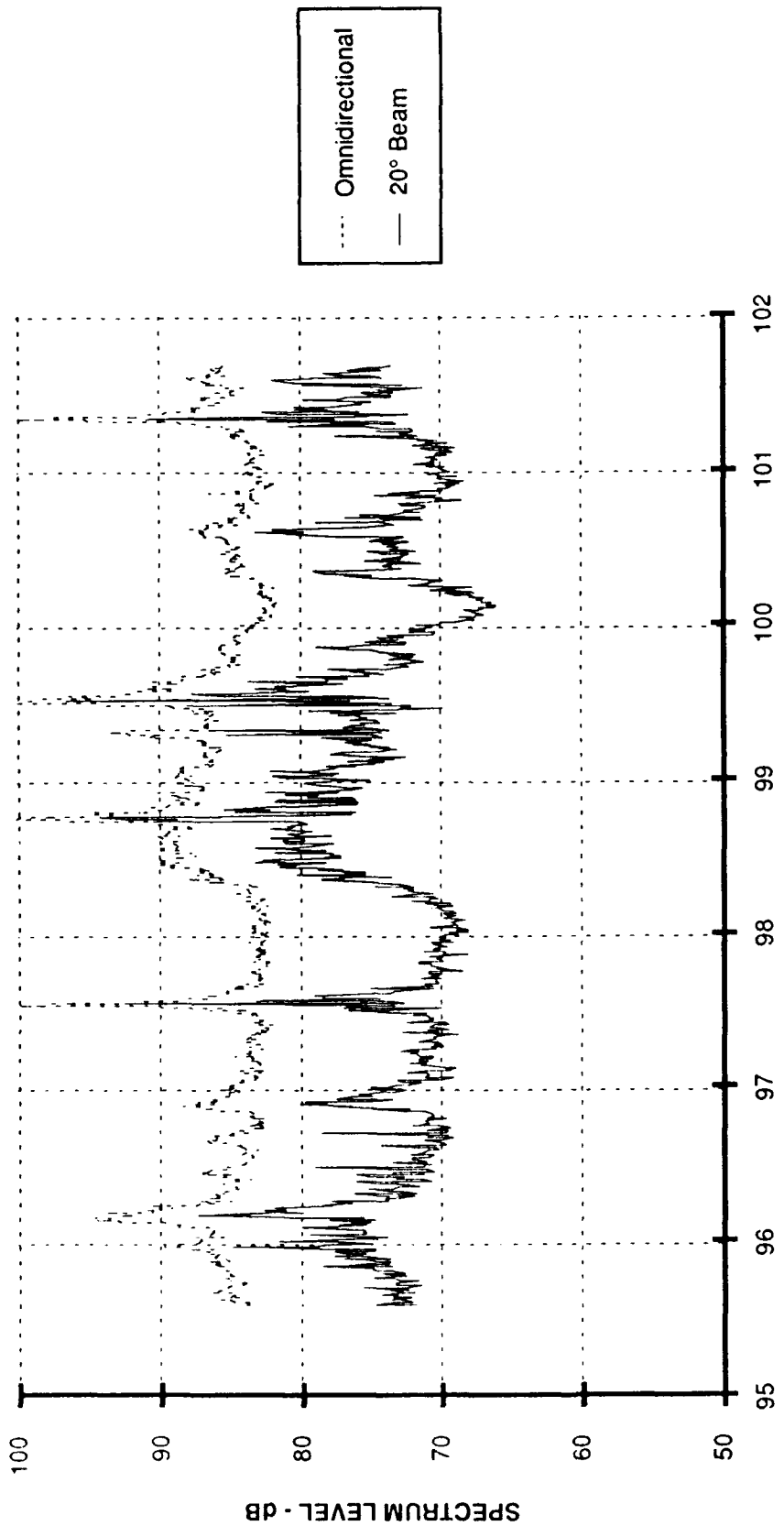

(e) 20° Beam

FIGURE 3.4 (cont'd)
BEAM NOISE TIMESERIES AT 55 Hz

ARL:UT
AS-90-931
CSP - DS
12 - 17 - 90

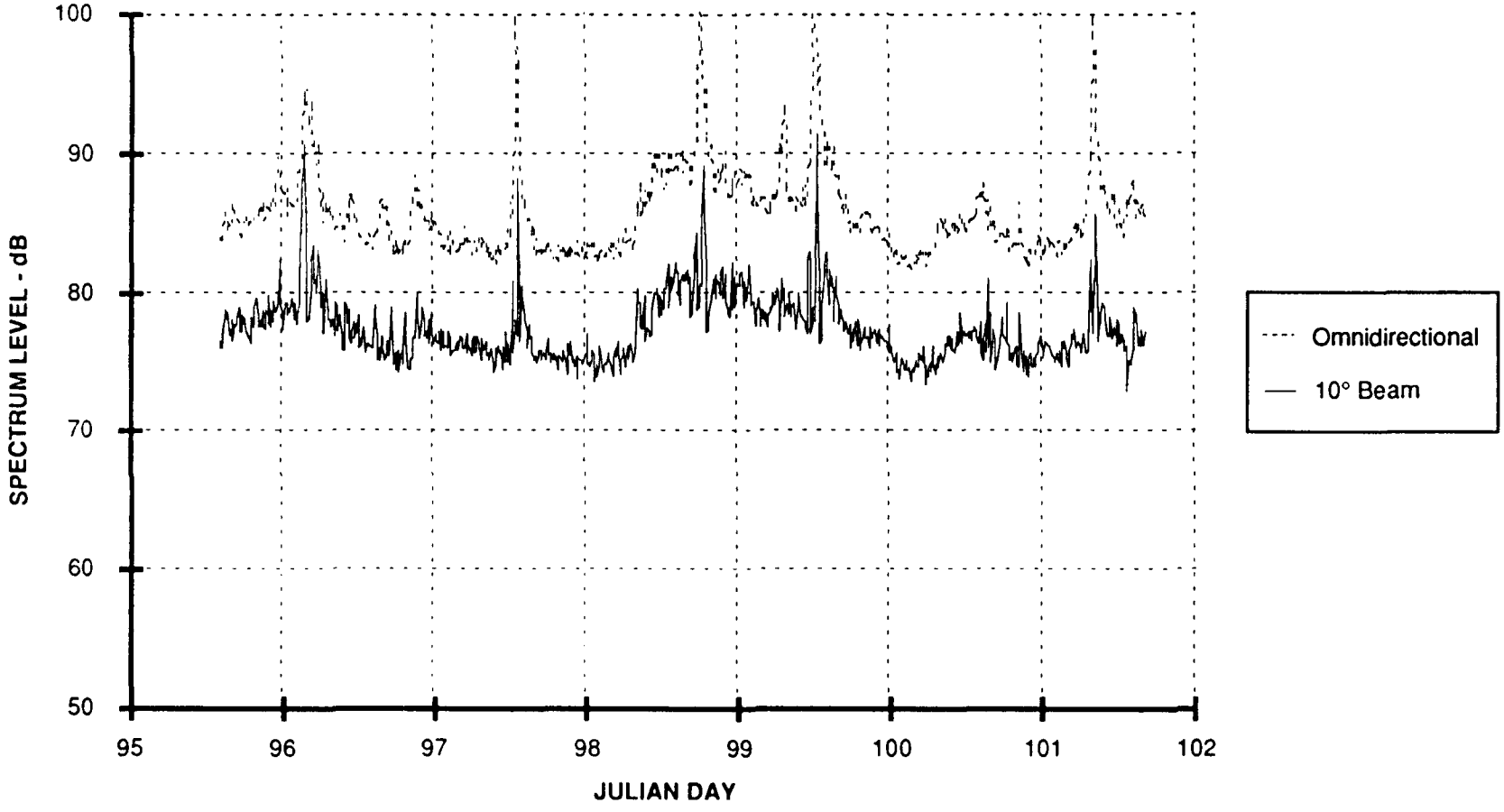

(f) 10° Beam

FIGURE 3.4 (cont'd)
BEAM NOISE TIMESERIES AT 55 Hz

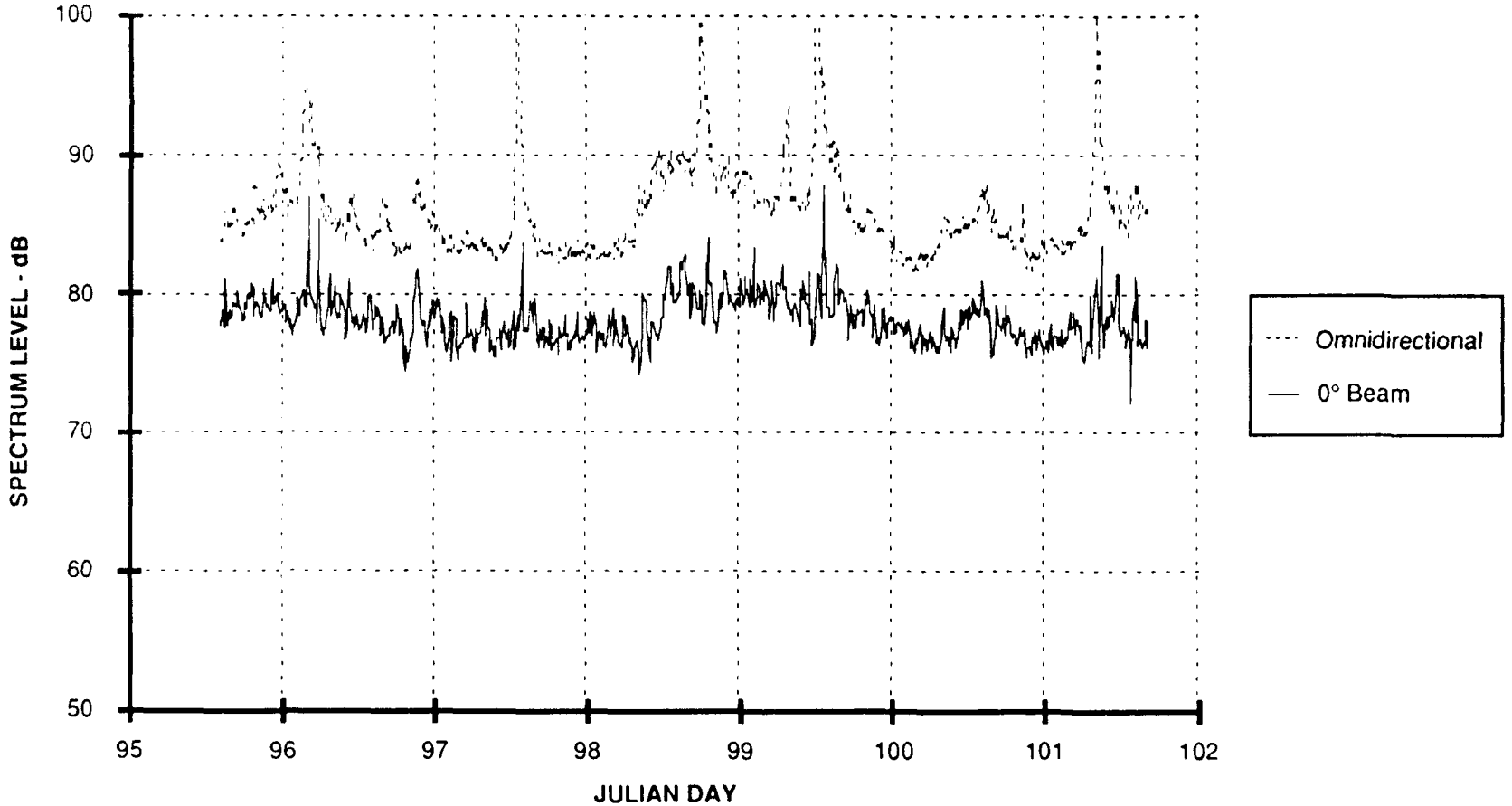

(g) 0° Beam

FIGURE 3.4 (cont'd)
BEAM NOISE TIMESERIES AT 55 Hz

3.2.1 High Angle Beams

The timeseries for the 90°, 60°, and 45° beams (Figs. 3.4(a)-(c)) are all quite similar in character. They show a background level near 58 dB which remains quite stable throughout the six day recording interval. This background level is interrupted by one long duration event (days 98-99) during which the noise level rises by approximately 4 dB and several events involving nearby shipping are observed. As noted above, due to sidelobe contamination the general character of the fluctuations in the beam noise for these three beams is very similar to that of the omnidirectional sensor. As a result, there is little to be learned from the background level on these beams. However, inspection of the local ship passage events reveals some effects of nearby ships on high angle noise. These will be discussed further in the following section.

During the elevated noise period (days 98 and 99), USNS ZEUS's radar detected nine ships moving through the area, several of which approached RAP range. The conjunction of these ships is probably the source of elevated noise levels during these two days. The similarity between the beam noise characteristics and the omnidirectional sensor during this time period suggests that the fluctuation in the high angle beam noise is due to sidelobe leakage rather than any measurable change in the high angle noise field.

3.2.2 Low Angle Beams

The beam steered at 30° above horizontal (Fig. 3.4(d)) exhibits the most severe fluctuations of all beams displayed in Fig. 3.4. During the events which cause increases in level, the 30° beam reaches levels nominally 10 dB greater than those of the higher angle beams. However, there are also time periods during which the 30° beam noise approaches the background level of the higher angle beams. These characteristics suggest that this beam is in a transition range. This beam is apparently capable of suppressing the distant traffic noise, as evidenced by the low levels achieved during quiet periods. However, this beam is more susceptible to shipping in the general area (within 100 nmi) than the higher angle beams.

The beam noise timeseries for steering angles of 10° and 20° are displayed in Fig. 3.4(e)-(f). These two beams are dominated by a combination of distant traffic and regional shipping. The 20° beam shows some similarity to the 30° beam in that it is capable of achieving some suppression of the distant shipping component.

3.2.3 Broadside Beam

The broadside beam (Fig. 3.4(g)) is the most stable beam, and the one least impacted by local ship passages, as expected. The median level for this beam is 77.5 dB, with a standard deviation of only 1.7 dB. The stability and level of the noise in this angular sector suggest that it is due to shipping traffic at long ranges, propagating along raypaths which graze the bottom at angles near horizontal. The low transmission loss associated with this angular sector allows contributions from long ranges, although Lloyd's mirror interference reduces the ability of shallow sources to couple into these paths.

Note that the individual ship CPA events which are quite obvious on the other beams appear to be somewhat suppressed on this beam. A Snell's law calculation shows that eigenrays which arrive at the bottom at a grazing angle of 0° are launched from the source at an angle of 6°. At 55 Hz, Lloyd's mirror effect (with the surface reflection coefficient equal to -1) will result in a loss of 11 dB for a source at 6 m depth. This at least partially accounts for the apparent suppression of local ship CPA events on the broadside beam.

3.2.4 Vertical Dipole

Figure 3.5 shows the beam noise timeseries for a dipole formed by taking the difference between the two elements of the array separated by 10 m. The dipole is normalized for unity on-axis response at 75 Hz, corresponding to half wavelength spacing. Although the noise gain associated with such an array is -3 dB in isotropic noise, the combination of the null in the beam pattern for horizontal angles and the low angle dominance of the noise field results in a median gain over the measurement period of -9.3 dB. At 55 Hz, with the dipole normalized as described, the signal gain for a plane wave arriving on axis is -0.8 dB. Hence, the median array gain for an ideal plane wave arriving from directly over the array would be 8.5 dB.

3.3 SUMMARY OF BEAM NOISE OBSERVATIONS

The beam noise observed during the VEDABS recording interval shows three distinct characteristics. Most prominent are the local ship passages which impact the noise in a fairly predictable manner during the period that the ship is within 20-40 nmi of the array. In addition to these events, there is a period of nominally two days during which several ships passed through the region within 100 nmi of the array and perturbed the

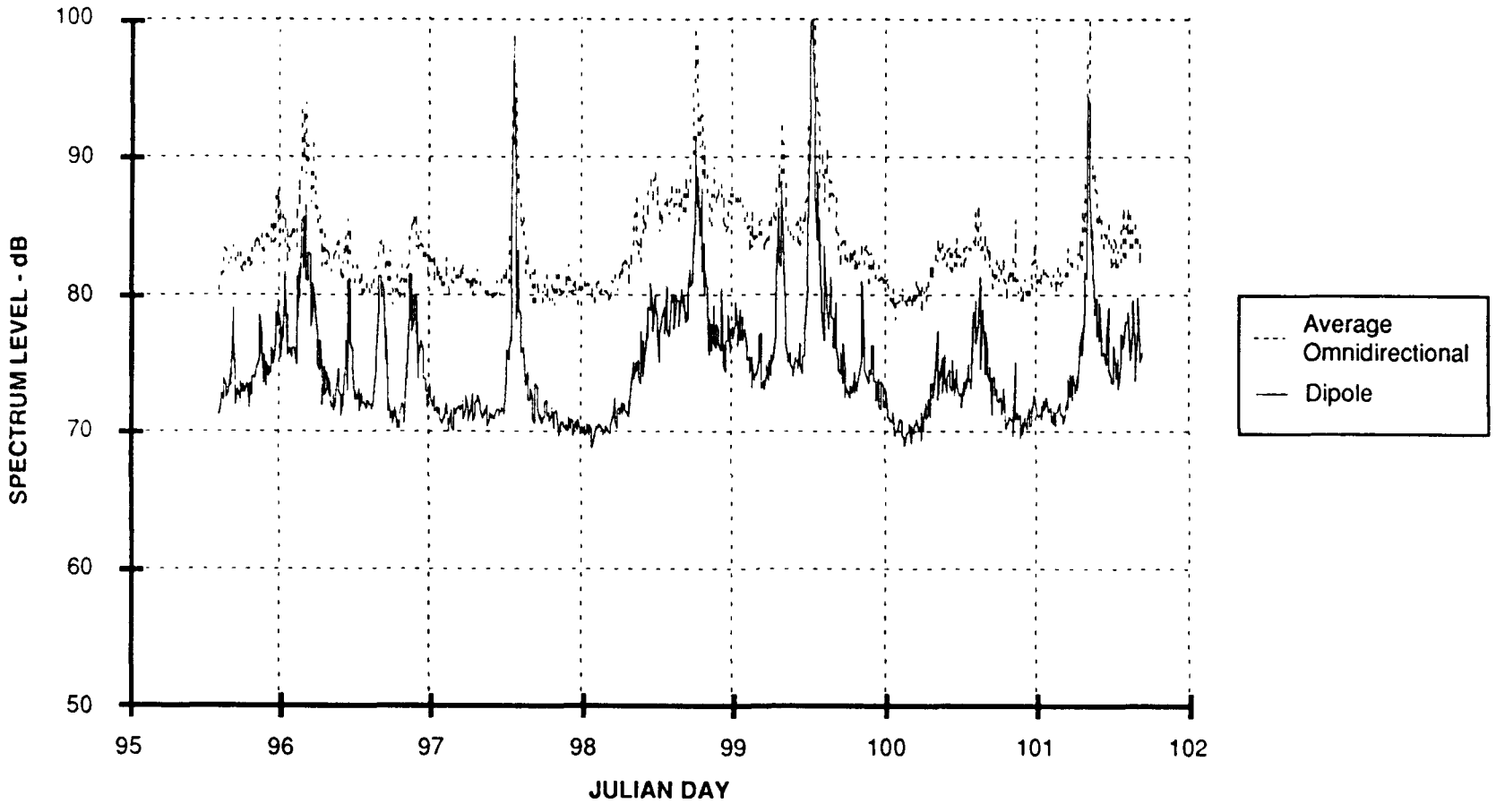

FIGURE 3.5
VERTICAL DIPOLE BEAM AND AVERAGE OMNIDIRECTIONAL ELEMENT TIMESERIES AT 55 Hz

ARL:UT
AS-90-934
CSP - DS
12 - 17 - 90

noise field. Finally, there are intervals such as day 97 during which a single ship passage is apparent; otherwise, the noise on this day appears to be dominated by long range shipping. The effect of these different conditions on the beam noise levels will be discussed in the sections below, followed by a summary and some general conclusions.

3.3.1 Discrete Ships

Those events due to nearby ship passages are easily identified in both the timeseries and the vertical directionality figures. The duration of individual ship events, combined with range estimates based on USNS ZEUS's radar, can provide some general insight concerning the range at which an individual ship is capable of impacting beam or omnidirectional noise. However, some caution is warranted since the sampling used in data reduction can cause the effect of the individual ships on beam noise to be somewhat obscured. On the surface the endfire beam has a footprint with a diameter of approximately 2 nmi at the -10 dB point. Beams between 30° and 60° have annular coverage on the surface with a width of nominally 1 nmi at the -10 dB points. Hence a ship moving at 10 kt will cross the endfire beam in less than 12 min, and may cross the annuli for beams between 30° and 60° in less time. Since the data are sampled at 1 min out of every 10 min, there is a significant probability that the time when the ship is on beam center will not be processed. This explains the fact that the observed peak levels for the individual ships do not necessarily agree with the omnidirectional level, as would be the case for ideal signal gain with the ship on beam center.

Each of the distinct shipping events results in an increase in beam noise level of 20-30 dB on the high angle beams, and has a nominal duration of 2 h. The effect is less pronounced as the beam steering angle approaches horizontal. The event at approximately 97/12 is a good example, since it occurs during a period when very few ships were in the area and noise levels were minimal, and it appears typical of several such events in the data. The radar log aboard USNS ZEUS indicates that this particular ship came within direct path range for the VEDABS array, and was traveling at approximately 9 kt. Noise timeseries for an omnidirectional element and several selected beams are displayed on an expanded time scale in Fig. 3.6.

For the beams steered at angles above 45°, the background noise level is perturbed for a period of only 1 to 2 h on either side of CPA, suggesting that high angle beam noise levels are relatively insensitive to an individual ship at ranges greater than 20-30 nmi. The beam steered at 30° shows the greatest sensitivity of all the beams displayed. Beam noise at

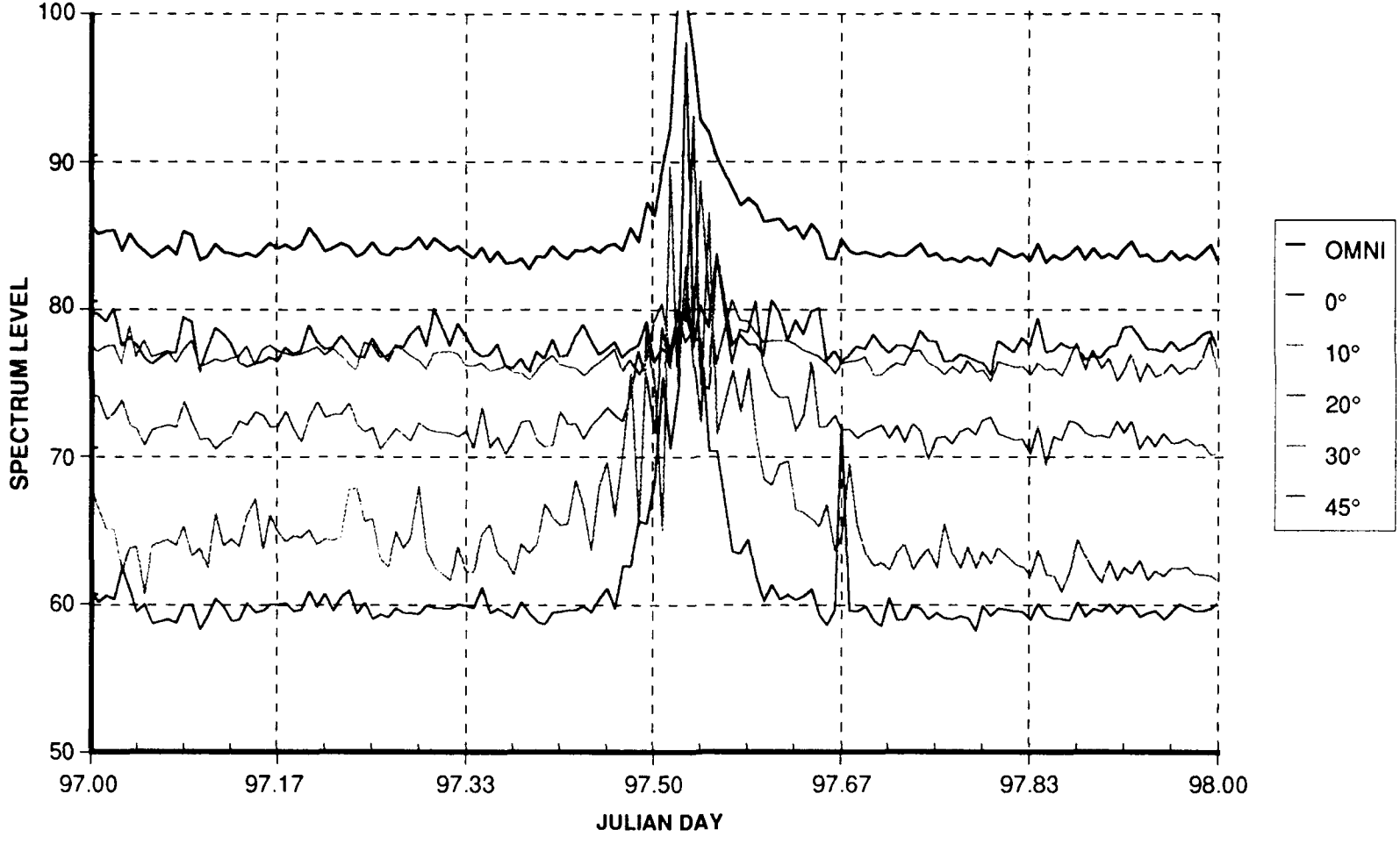

FIGURE 3.6
BEAM NOISE TIMESERIES AT 55 Hz SURROUNDING A MERCHANT SHIP PASSAGE

ARL:UT
AS-90-935
CSP - DS
12 - 17 - 90

30° is influenced for a period of 3-4 h, indicating that a single ship within 50 nmi of the array may influence beam noise at this angle. At the lower angles, the apparent duration of the event is diminished by the higher background level on these beams. The broadside beam shows little effect due to this ship because of a combination of high background level and Lloyd's mirror interference.

3.3.2 Intermediate Range Shipping

The data suggest that a single ship at ranges greater than 50 nmi is unable to dominate the noise field. However, a number of ships in the intermediate range interval of 50-100 nmi may have a significant impact on the beam noise for beams steered between 10° and 30°. In order to examine these conditions more carefully, Table 3.1 is presented summarizing beam and omnidirectional noise levels for four periods of a few hours duration surrounding 98/0, 98/12, 99/0, and 100/3. Levels marked with an asterisk in the table are contaminated with low angle contributions through the sidelobes and should be considered upper bounds on achievable beam noise.

The first and last time periods in Table 3.1 are representative of the noise directionality during relatively quiet periods. The middle two time periods are representative of conditions with several ships within nominally 100 nmi of the array. In order to assess the contributions of the intermediate range ships, we will compare the directionality of the two quiet periods with the other two.

TABLE 3.1
BEAM AND OMNIDIRECTIONAL NOISE LEVELS DURING FOUR TIME PERIODS

Omni-directional (deg)	98/0	98/12	99/0	100/3
	83	89	89	82
0	77	80	80	77
10	76	80	80	75
20	70	80	79	68
30	61*	77	72	59*
45	58*	62*	61*	57*
60	58*	63*	63*	57*
90	58*	63*	62*	57*

*Contaminated with low angle contributions through the sidelobe.

From Table 3.1, the intermediate range shipping results in a 6 dB increase in omnidirectional level. The 0° and 10° beam levels are increased by 3-5 dB, while the 20° beam shows an increase of 10-11 dB. The impact on the 30° beam is more difficult to ascertain, since this beam is sidelobe limited for the quieter time periods. However, the increase is at least 13-16 dB, and is clearly larger than on the lower angle beams. The beams steered at 45° and above are sidelobe limited for all four periods and show increases similar to those of the omnidirectional sensor. These measurements suggest that the intermediate range shipping has a substantial influence on beams in the 10-30° angular sector.

3.3.3 Summary of Shipping Observations

The measurements described above lead to several conclusions concerning environmental mechanisms which govern the vertical structure of the ambient noise field at low frequencies near the bottom. These are listed below.

(1) The maximum range at which an individual ship is able to significantly impact the noise field at angles above 45° is less than 30 nmi. Sound propagating at these steep angles experiences frequent high loss bottom interaction. At 30°, where ray cycle distances are longer and the bottom loss is slightly lower, the range at which a single ship is able to impact beam noise approaches 50 nmi.

(2) The noise field at angles between 10° and 30° is apparently quite sensitive to shipping traffic which is within nominally 100 nmi of the array.

(3) The noise field at angles below 10° is determined primarily by distant shipping traffic, and appears to be highly stationary. However, significant increases in intermediate range shipping can raise the noise at low angles by a few decibels.

An interesting footnote to the conclusions summarized above is that the TAGEX 87 environment is an area with low bottom loss. In thin sediment areas with higher bottom loss at low grazing angles, we would expect to see an even greater range limiting effect. Testing this hypothesis was the objective of the OUTPOST SUNRISE experiment conducted by the ONR ASW Environmental Acoustic Support Program. Results are documented in Mitchell and Levinson.[13]

4. MODEL CALCULATIONS

In this section, we will discuss two approaches to modeling the spatial structure of the ambient noise field. One is a standard model known as ANDES (ambient noise directionality estimation system) developed under support of the ONR ASW Environmental Acoustic Support Program, and used in Fleet performance prediction as well as in research environments. The other is a research model assembled at ARL:UT to investigate specific aspects of the TAGEX 87 data set. Finally, we will show some calculations to describe the angular dependence of noise from a single ship as a function of range.

4.1 ANDES CALCULATIONS

Several models are available which support calculation of the vertical directionality of the ambient noise field. One which has been exercised frequently is the ANDES[14] model. ANDES calculates directionality by using the ASTRAL transmission loss model to propagate energy from shipping and wind noise sources. The distribution of shipping noise sources is derived from the HITS database.

Figure 4.1 shows a comparison of ANDES predicted beam noise levels with the measured beam noise reproduced from Fig. 3.3. The ANDES calculation of the vertical directionality of the noise field was produced for summer conditions, with local wind speed at 15 kt. Beam noise levels were estimated by convolving the directionality estimate from ANDES with the beam pattern of the array. Comparison of the ANDES calculation with the measurements is best done on the basis of the angular sectors discussed in the preceding sections, since this will allow us to discuss the differences in terms of the dominant mechanisms contributing to the noise field in that sector. Because ANDES uses the HITS shipping database, which represents average shipping concentrations, it is probably most appropriate to compare the ANDES calculation with the median of the measurements.

In the sector between $\pm 10°$, the ANDES estimate falls generally within 2 dB of the median beam noise. Since this sector appears to be dominated by the effects of long range shipping arriving via eigenrays which experience very little bottom interaction, good agreement suggests that the ship source levels and shipping density database used in the model are sound.

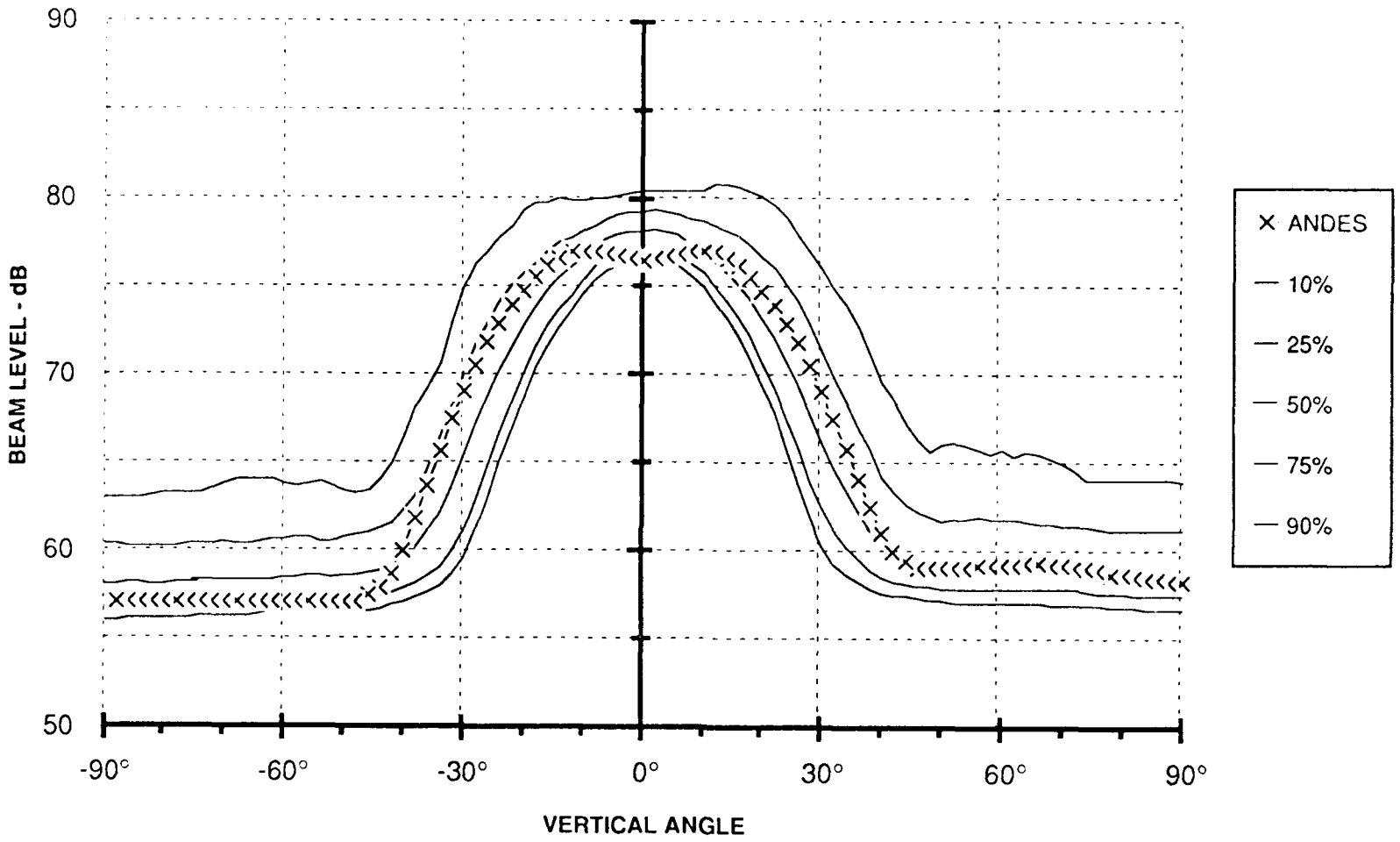

FIGURE 4.1
COMPARISON OF ANDES PREDICTIONS WITH MEASURED BEAM NOISE

At angles between 10° and 40° off horizontal, the discrepancy between ANDES calculations and the measured median remains less than 3 dB for the positive angles, and up to 4 dB for the negative angles. This sector would appear to offer the most difficult estimation problem since it is governed by a complicated interplay between intermediate range shipping and the dependence of bottom loss on grazing angle. Hence, the generally good agreement between the model and the data in this sector is quite encouraging.

The steeper angles in the measurements are dominated by sidelobe leakage, which is also represented in the model calculations, since the ANDES produced directionality is convolved with the beam pattern. However, in this case, the accuracy of the model prediction depends on the accuracy with which the average sidelobe level is known. The disagreement between the model and the data is excellent for the positive angles, and within 2 dB for the negative angles.

Generally speaking, the level of agreement between ANDES directionality estimates and the measured median is impressive, and also suggests that the shipping densities and bottom loss characteristics of the region are well described in the databases.

4.2 RAY TRACE CALCULATIONS BASED ON OBSERVATIONS OF LOCAL SHIPPING

The ANDES calculations described above yield a good representation of the static, or median, characteristics of the noise field. In order to examine the effect of shipping moving through the area, and to estimate the extent to which the observed characteristics of the noise field could be explained in terms of intermediate range shipping, a simple dynamic model was developed which could accept as input the tracks of local ships. As mentioned above, USNS ZEUS maintained station at approximately 12 nmi from the VEDABS site throughout the recording interval. During this period, logs were maintained of shipping which passed within radar range of approximately 25 nmi. These ships were used as the basis for a ray trace calculation of the vertical directionality of the noise field.

The calculations were based on an assumption that the ships tracked by USNS ZEUS's radar maintained their course and speed after leaving the radar coverage area. Since the site was far removed from any obstacles which might dictate course changes, this assumption appears sound. Source levels assigned to the ships were similar to those used in ANDES calculations. The source levels were between 165 and

175 dB//μPa^2/Hz, assigned on the basis of the ship's size, when available. If no indication of size was available, a level between 165 and 175 dB was assigned at random. Source levels were increased by 3 dB on the outbound leg to account for the apparent aspect dependence observed in the data. At 10 min intervals along each ship's track, a set of eigenrays was found. Transmission loss was calculated for each ray and the contributions of each ship were added to the received noise field, properly weighted by the transmission loss, and distributed in vertical angle according to the eigenray arrival angle. The resulting directionality was convolved with the beam pattern to produce an estimate of beam noise level versus time.

The resulting picture of noise field directionality is shown in Fig. 4.2. The figure shows fluctuations similar in character to those found in the data. However, more importantly, the model calculations indicate that much of the energy between 10° and 30° can be accounted for on the basis of a modest number of ships distributed within 100 nmi of the array. The model fails to accurately represent the very low angle component of the field illustrated by the 0° beam data from Fig. 3.4(c). As pointed out above, this component of the field is attributable to distant shipping sources which are not included in the model.

The individual events related to ship passages in the model calculation generally have a longer rate of decay than the data. However, the model is generally in agreement with the data in predicting a relatively limited range of influence for a surface ship on the noise field at angles above 30°.

4.3 BEAM TRANSMISSION LOSS CALCULATIONS

Both the model calculations and the beam noise measurements indicate that surface ships passing in the vicinity of the array influence beam noise levels only over a relatively short range interval of up to 30 nmi for the beams steered above 20°. For example, the ship which passes near the array at 98/18 generates multipath structure visible in the beam noise. However, only one arrival order is seen on the approach leg, while only two are clearly visible on the departing leg. In order to gain a better understanding of this range limiting effect, a ray trace calculation of transmission loss in angular windows was performed to determine the loss associated with energy arriving from the ship in various beams. The results of this calculation are shown in Figs. 4.3(a)-(c).

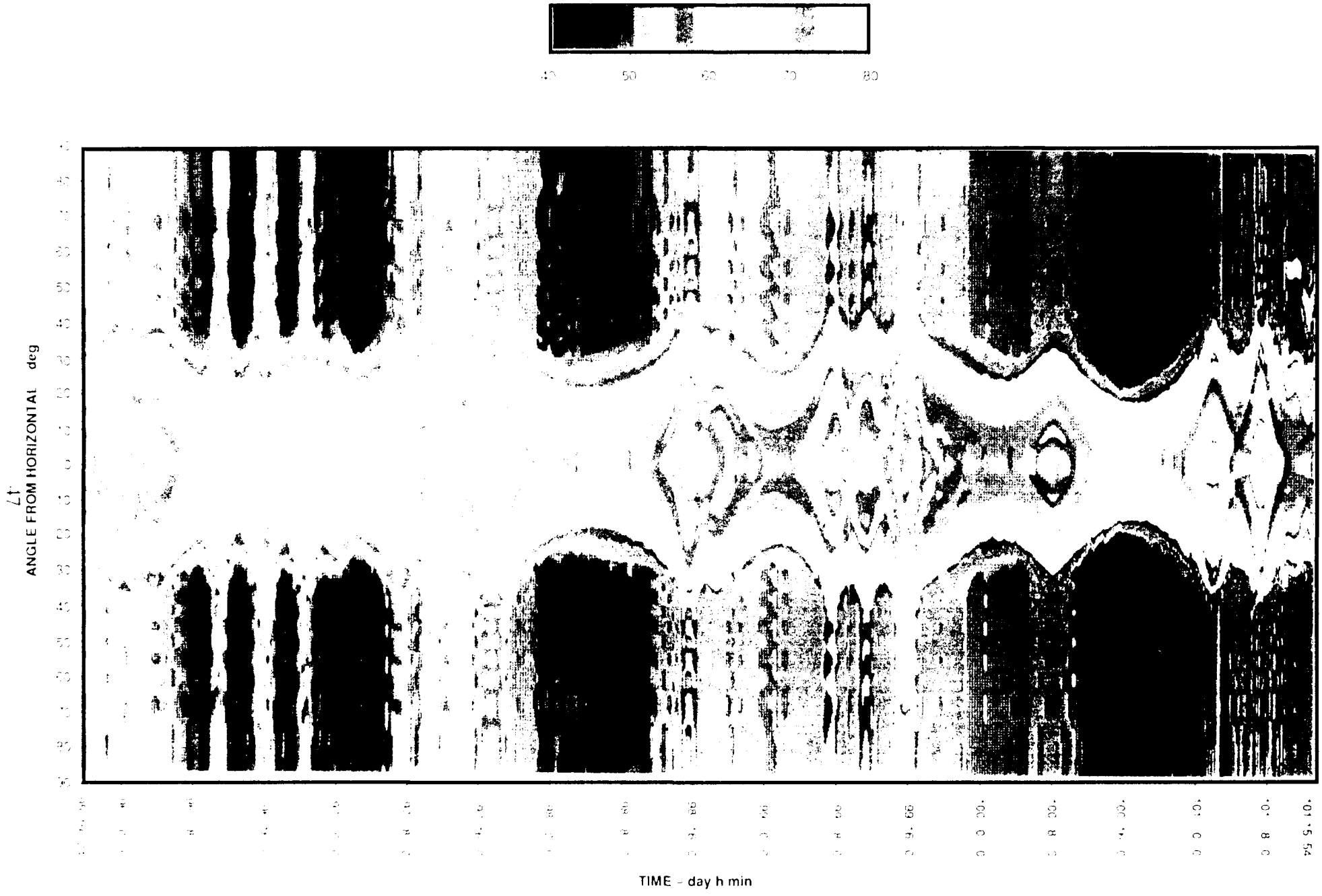

FIGURE 4.2
MODELED TIME DEPENDENCE OF VERTICAL DIRECTIONALITY

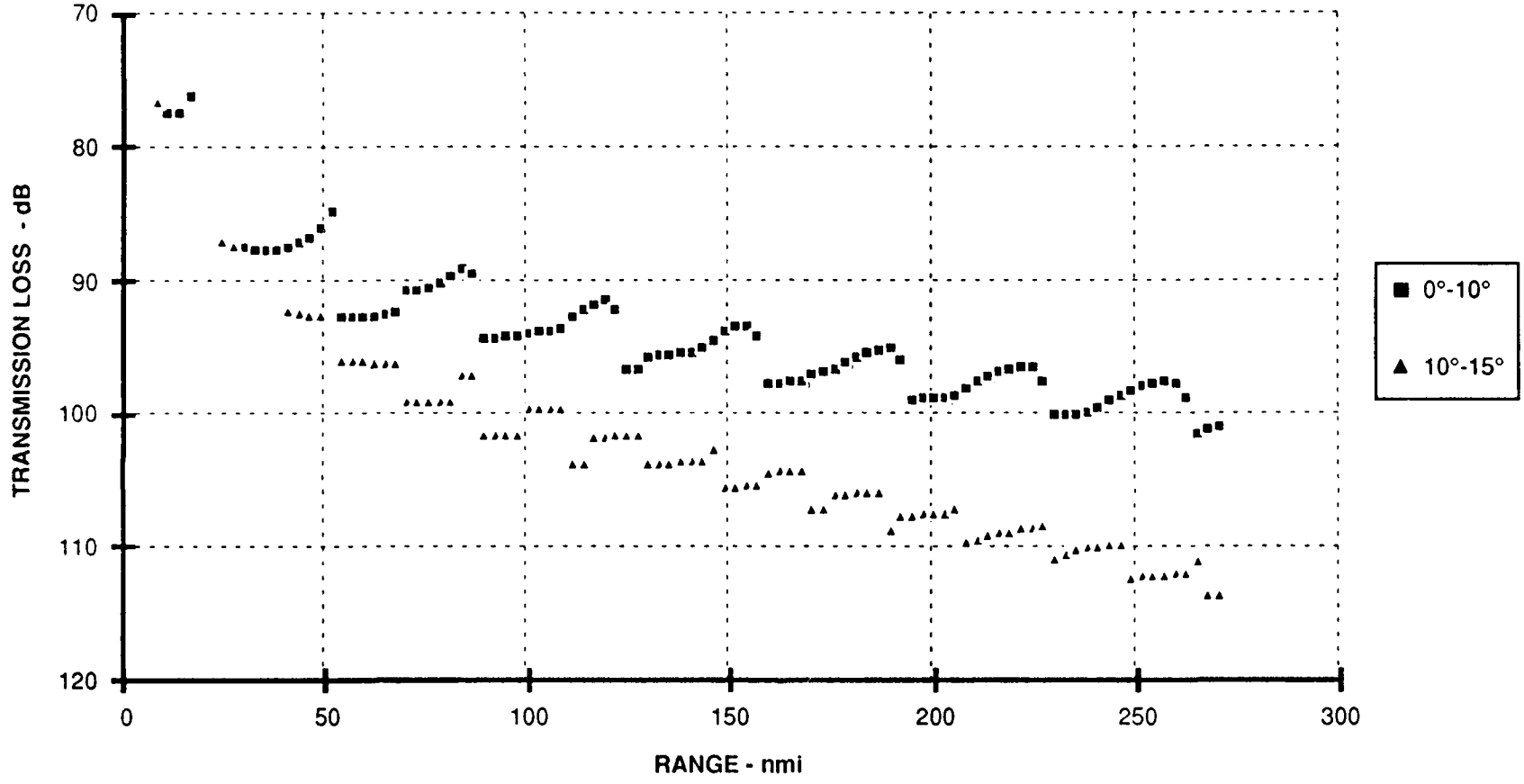

(a) VERTICAL ANGLE SECTORS 0°-10° AND 10°-15°

FIGURE 4.3
RAY TRACE CALCULATIONS OF TRANSMISSION LOSS AT 50 Hz
(BOTTOMED RECEIVER, 5 m SOURCE DEPTH)

ARL:UT
AS-90-938
CSP - DS
12 - 17 - 90

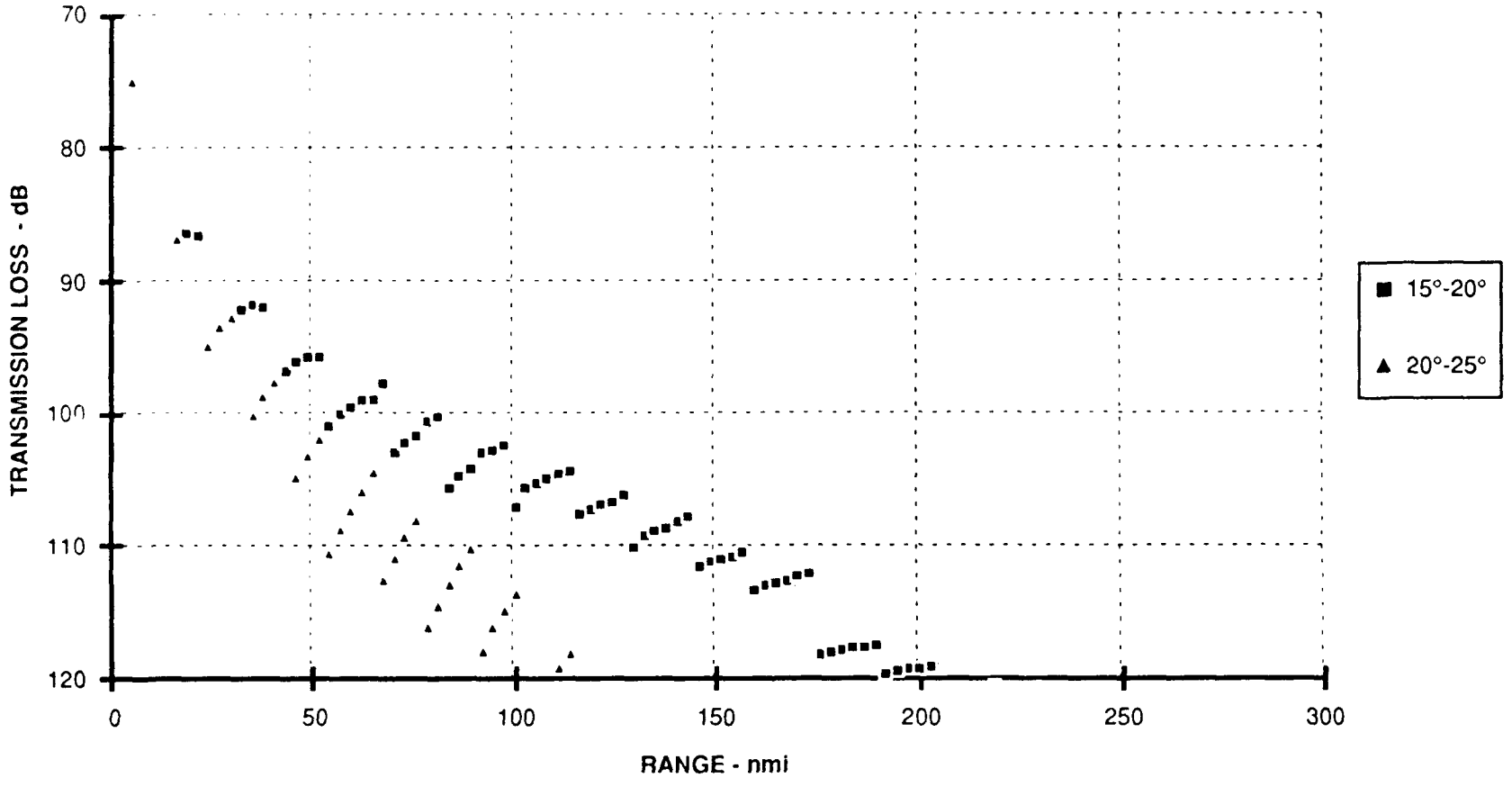

(b) VERTICAL ANGLE SECTORS 15°-20° AND 20°-25°

FIGURE 4.3 (cont'd)
RAY TRACE CALCULATIONS OF TRANSMISSION LOSS AT 50 Hz
(BOTTOMED RECEIVER, 5 m SOURCE DEPTH)

ARL:UT
AS-90-939
CSP - DS
12 - 17 - 90

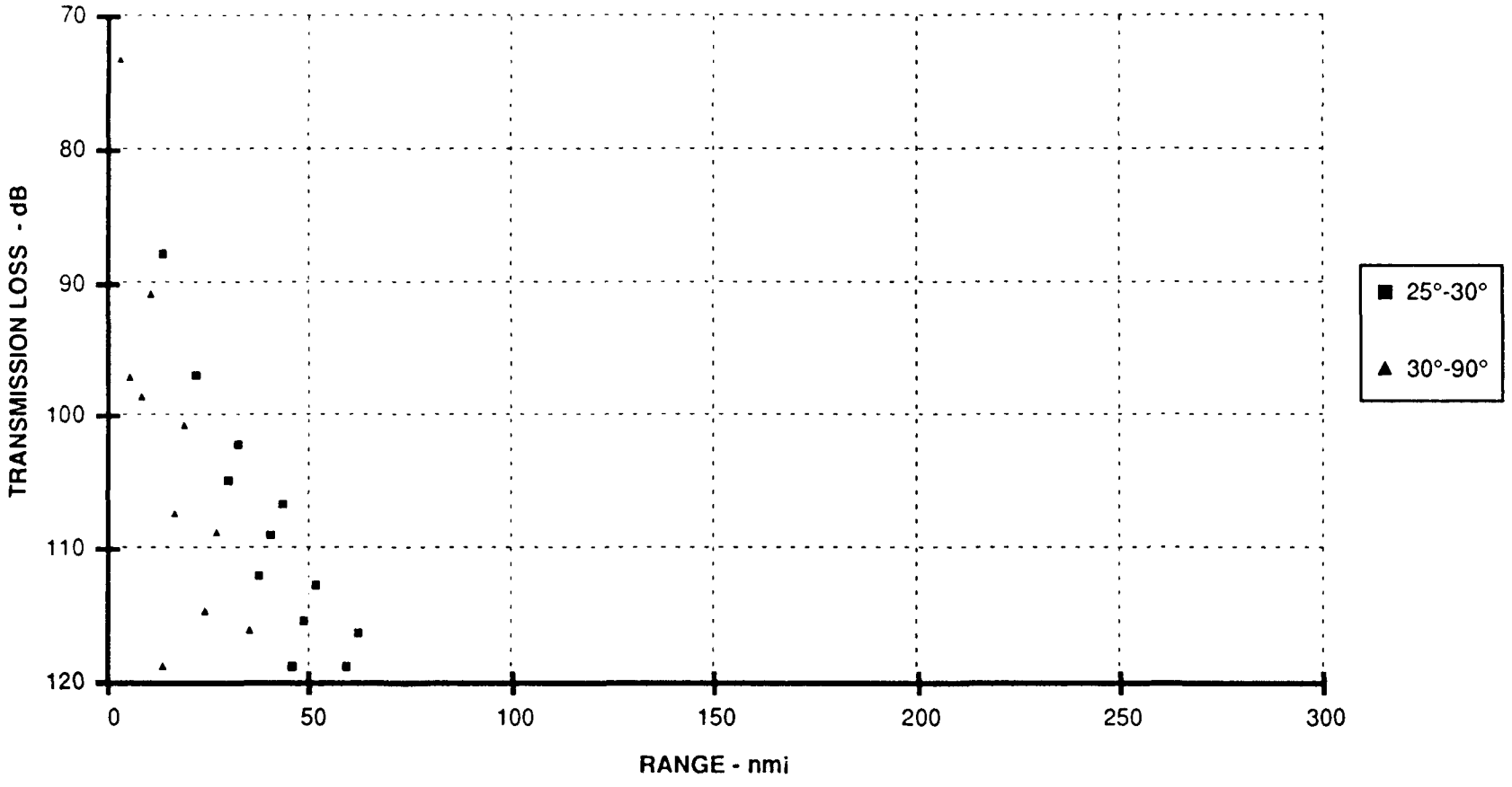

(c) VERTICAL ANGLE SECTORS 25°-30° AND 30°-90°

FIGURE 4.3 (cont'd)
RAY TRACE CALCULATIONS OF TRANSMISSION LOSS AT 50 Hz
(BOTTOMED RECEIVER, 5 m SOURCE DEPTH)

ARL:UT
AS-90-940
CSP - DS
12 - 17 - 90

The calculations in Fig. 4.3 are for a 5 m source depth and a bottomed receiver. The archival summer sound speed profile for the TAGEX 87 site was used to obtain estimates of transmission loss versus range for rays arriving at the receiver within vertical angular windows. For these calculations, the energy associated with all the eigenrays arriving within the specified sector was summed incoherently to determine transmission loss.

Figure 4.3(a) shows that transmission loss in the 10-15° sector is nominally 100 dB at 100 nmi, and approaching 110 dB at 200 nmi. Examination of Fig. 4.3(b) shows that in the 15-20° sector, the figures are 105 dB and 120 dB, respectively. At 50 nmi, transmission loss for the 20-25° sector is approaching 100 dB, and increasing rapidly. These figures confirm the range limiting effect for individual ships observed in the data. Another effect observed in the data is that the noise field in the sector between 10° and 30° is dominated by shipping within nominally 100 nmi of the array. These transmission loss calculations do not account for the increased surface area with range, and the resulting increase in the number of ships. However, they do provide some indication of the dramatic range dependence of transmission loss for beams steered at angles above horizontal.

4.4 RANGE DEPENDENCE OF BEAM NOISE CONTRIBUTIONS

In order to more fully understand the range intervals which dominate the beam noise at various vertical angles, the ANDES model was used. In this case, the beam noise calculation was modified so that contributions from shipping sources within an exclusion radius of the site could be eliminated. Hence, the calculation is of the form

$$bn(\theta_0, r_e) = \int_{r_e}^{\infty} \int_{-\pi/2}^{\pi/2} b(\theta, \theta_0) n(\theta, r) d\theta dr \qquad (4.1)$$

where $n(\theta,r)$ is the noise contribution at vertical angle θ from sources at range r, $b(\theta,\theta_0)$ is the beam pattern, and r_e is the exclusion radius. The result of the calculation for various vertical angles is shown in Fig. 4.4.

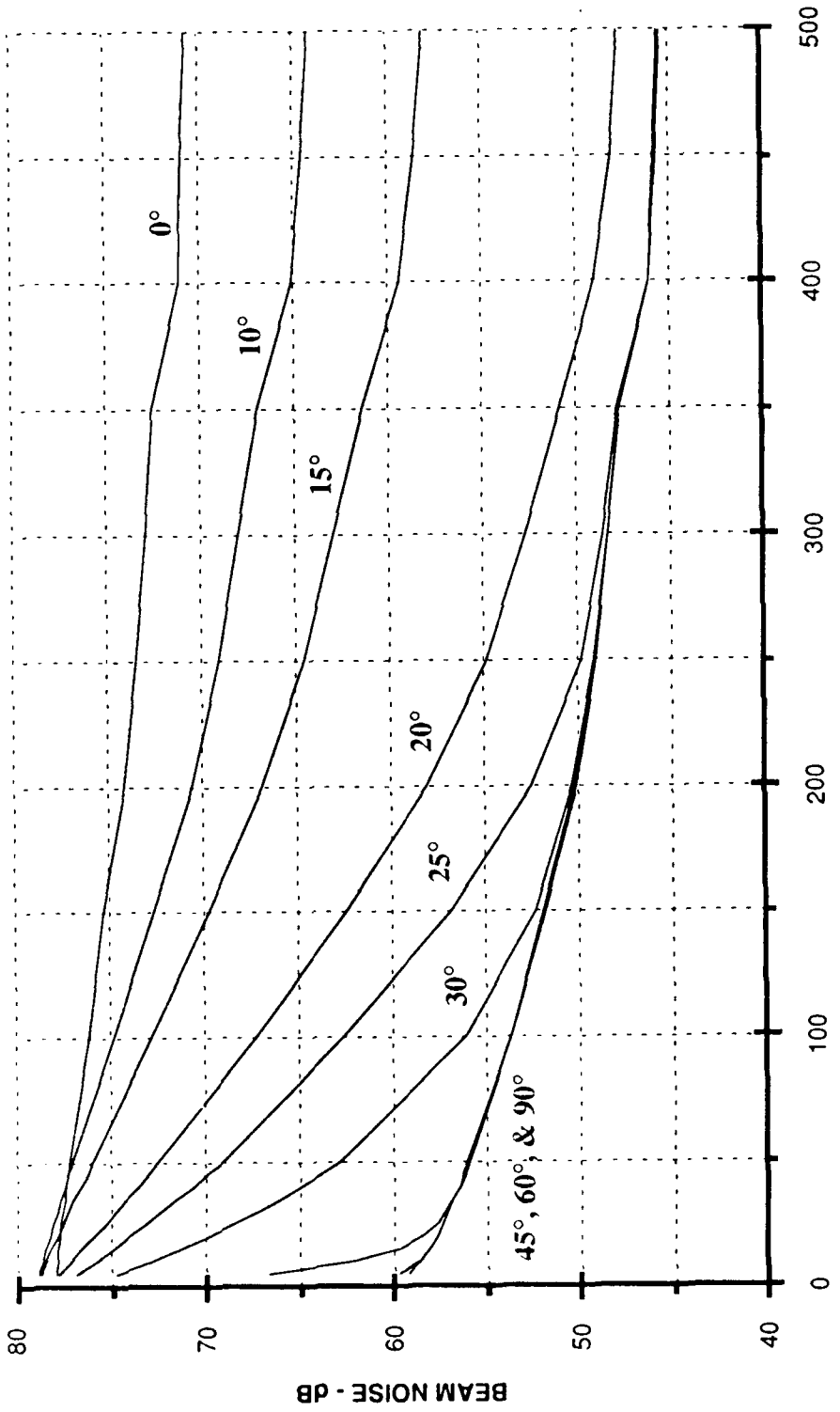

FIGURE 4.4
ANDES CALCULATION OF BEAM NOISE LEVEL versus RADIUS OF EXCLUSION

ARL:UT
AS-90-941
CSP - DS
12 - 17 - 90

The figure illustrates the range intervals which dominate the noise at different vertical angles. The steeper angles are more dominated by short range sources, and hence the rate at which the beam noise decreases with increasing r_e is quite rapid. The shallower grazing angles are more dominated by long range sources, and hence beam noise for these beams shows a very slow rate of decrease as the exclusion range is increased.

Examination of the beam steered at 30° shows that when the exclusion range is 50 nmi, beam noise has been reduced from 75 dB to 63 dB. Exclusion of shipping sources within 100 nmi further reduces the beam noise level to 56 dB. Clearly, the model calculations support the conclusion that this beam is dominated by shipping within 100 nmi of the site. Similar statements apply to the beam steered at 25°, with the noise only slightly less dominated by shipping within 100 nmi. On the other hand, the beam steered at 15° is reduced to a level of 60 dB only for exclusion ranges in excess of 375 nmi.

5. SUMMARY

The most important conclusion to be drawn from this work is a modified understanding of the mechanisms which determine the vertical spatial structure of the ambient noise field near the ocean bottom. The contribution of distant traffic noise has been shown to be confined to very low angles ($-10° \leq \theta \leq 10°$) in this data set. Between the angles of 10° and 30°, the noise is heavily influenced by shipping at ranges of up to 50-100 nmi. The portion of the angular spectrum steeper than 30° is dominated by sea state noise except during periods when a ship is within 30-50 nmi of the array.

This assessment of vertical spatial structure is based on data from a deep basin site with low bottom loss typical of such sites in the Atlantic. The shipping density of 1-2 ships/deg^2 predicts that, on average, roughly five ships are expected within 50 nmi of the site. This is reasonably consistent with USNS ZEUS's observations. An area with greater shipping density would experience fewer intervals when distant shipping noise was visible on beams steered below 30°. However, areas with greater bottom loss, such as thinly sedimented Pacific basins, will experience greater limitation of noise arriving via bottom bounce paths from intermediate range shipping.

Model calculations of noise field directionality, beam noise, and range dependence of sources contributing to beam noise levels have been shown to be consistent with the data, and with the observations described above. However, at present, no database is available that contains shipping locations sufficiently complete to support a more detailed analysis of the impact of shipping distribution on vertical directionality.

The data and the model calculations suggest that the noise field in the vertical sector between 10° and 30° may be characterized by strong azimuthal anisotropy due to a relatively limited number of contributing noise sources. At present, a suitable data set to explore this conjecture is non-existent.

REFERENCES

1. V. C. Anderson, "Arrays for the Investigation of Ambient Noise in the Ocean," J. Acoust. Soc. Am. 30, 470-477 (1958).

2. J. Stone, "Problems Associated with the Measurement of Ambient Noise Directivity by Means of Linear Additive Arrays," J. Acoust. Soc. Am. 34, 328-333 (1962).

3. B. A. Becken, "The Directional Distribution of Ambient Noise in the Ocean," SIO Reference 61-4, Marine Physical Laboratory, Scripps Institution of Oceanography, The University of California, San Diego, 7 March 1961.

4. P. Rudnick and E. D. Squier, "Fluctuations and Directionality in Ambient Sea Noise," J. Acoust. Soc. Am. 41, 1347-1351 (1967).

5. C. A. Foster, "Ambient Sea Noise Directivity," J. Acoust. Soc. Am. 34, 1986 (A) (1962).

6. E. H. Axelrod, B. A. Schoomer, and W. A. Von Winkle, "Vertical Directionality of Ambient Noise in the Deep Ocean at a Site near Bermuda," J. Acoust. Soc. Am. 37, 77-83 (1965).

7. G. R. Fox, "Ambient Noise Directivity Measurements," J. Acoust Soc. Am. 36, 1537-1540 (1964).

8. V. C. Anderson, "Variation of the Vertical Directionality of Noise with Depth in the North Pacific," J. Acoust. Soc. Am. 66, 1446-1452 (1979).

9. J. Lynch and K. E. Hawker, "A Statistical Description of Bottom Loss and Propagation Loss for the North Atlantic and Eastern Pacific Oceans," Applied Research Laboratories Technical Report No. 82-26 (ARL-TR-82-26), Applied Research Laboratories, The University of Texas at Austin, 3 May 1982.

10. N. Yen, "Ambient Sea Noise Directionality: Measurement and Processing," J. Acoust. Soc. Am. 62, 1176-1188 (1978).

11. N. Yen, "Analytic Expansion Techniques for Ambient Noise Directionality Determination," J. Acoust. Soc. Am. 66, 494-496 (1979).

12. J. S. Hanna, Science Applications International Corporation, private communication.

13. S. K. Mitchell and S. J. Levinson, "OUTPOST SUNRISE VEDABS Acoustic Data Report," Applied Research Laboratories Technical Report No. 90-28 (ARL-TR-90-28), Applied Research Laboratories, The University of Texas at Austin, September 1990.

14. W. W. Renner, "Ambient Noise Directionality Estimation System (ANDES) Technical Description," SAIC Technical Report No. SAIC-86/1645, Science Applications International Corporation, McLean, Virginia, June 1986.

1 November 1990

DISTRIBUTION LIST FOR
ARL-TR-90-37
TECHNICAL REPORT UNDER
CONTRACT N00024-86-C-6134, TASK 1, PROJECT 10, and
CONTRACT N00039-88-C-0043, TD Nos. 01A002 and 01A003

Copy No.

Commander
Space and Naval Warfare Systems Command
Department of the Navy
Washington, D.C. 20363-5100

1 Attn: CAPT K. Evans (PD80)
2 L. Parish (PMW181T)
3 C. Andriani (PMW183T)
4 R. Mitnich (PMW183-33)
5 CDR W. Hatcher (PMW184T)
6 CDR D. Liechte (PMW184-3)
7 G. Hetland (PMW183-34)
8 L. Fabian (PMW183-4)
9 W. Richter (PMW183-41)

Office of the Deputy Assistant Secretary of the Navy
Antisubmarine Warfare Programs
Department of the Navy
Washington, DC 20350-1000

10 Attn: A. Bisson
11 CDR D. Backes

Office of the Chief of Naval Operations
Department of the Navy
Washington, D.C. 20350-2000

12 Attn: J. Schuster (OP-02T)
13 CAPT F. Crawford (OP-24)

Office of the Chief of Naval Operations
Naval Observatory
34th and Massachusetts Ave.
Washington, D.C. 20390

14 Attn: R. Winokur (Code 096T)

Office of the Chief of Naval Research
Department of the Navy
Arlington, VA 22217-5000

15 Attn: R. Feden (Code 125)
16 K. Dial (Code 125)

Distribution list for ARL-TR-90-37 under Contract N00024-86-C-6134, Task 1, Project 10 and Contract N00039-88-C-0043, TD Nos. 01A002 and 01A003 (cont'd)

Copy No.

Office of Naval Research Field Detachment
Stennis Space Center, MS 39529-5000
17 Attn: E. Chaika (Code 125)
18 B. Blumenthal (Code 125)

Office of the Chief of Naval Research
Office of Naval Technology
Department of the Navy
Arlington, VA 22217-5000
19 Attn: C. Votaw
20 R. Doolittle
21 T. Goldsberry

Defense Advanced Research Projects Agency
1400 Wilson Blvd.
Arlington, VA 22209
22 Attn: C. Stuart

Commander
Naval Air Systems Command
Department of the Navy
Washington, DC 20361-7121
23 Attn: E. Benson (PMA 264)

Director
Naval Research Laboratory
Washington, DC 20375-5000
24 Attn: D. Bradley (Code 5100)
25 O. Diachok (Code 5120)
26 W. Kuperman (Code 5160)

Commanding Officer
Naval Ocean Systems Center
San Diego, CA 92152-5000
27 Attn: H. Bucker (Code 541)
28 H. Schenck (Code 701)
29 D. Hanna (Code 705)
30 C. Persons (Code 732)
31 K. Rogers (Code 714)
32 D. Barbour (Code 732)

Distribution list for ARL-TR-90-37 under Contract N00024-86-C-6134, Task 1, Project 10 and Contract N00039-88-C-0043, TD Nos. 01A002 and 01A003 (cont'd)

Copy No.

Commanding Officer
Naval Oceanographic and Atmospheric Research Laboratory
Stennis Space Center, MS 39529-5000
33 Attn: B. Adams (Code 110A)
34 J. Matthews (Code 222)
35 R. Wagstaff (Code 425)

Commanding Officer
Naval Oceanographic Office
Stennis Space Center, MS 39522-5000
36 Attn: W. Jobst (Code 7300)
37 R. Hecht (Code 7310)

Commanding Officer
Naval Air Development Center
Warminster, PA 18974
38 Attn: L. Allen
39 C. Bartberger
40 B. Steinberg (Code 5031)

Officer in Charge
Naval Underwater Systems Center
New London Laboratory
New London, CT 06320
41 Attn: B. Cole (Code 33A)
42 F. DiNapoli
43 P. Herstein (Code 33A3)
44 W. Carey (Code 33A)

Superintendent
Naval Postgraduate School
Monterey, CA 93940
45 Attn: Library

Commanding Officer
Naval Technical Intelligence Center
4301 Suitland Rd.
Washington, D.C. 20395-5020
46 Attn: B. Rule

Distribution list for ARL-TR-90-37 under Contract N00024-86-C-6134,
Task 1, Project 10 and Contract N00039-88-C-0043, TD Nos. 01A002 and 01A003
(cont'd)

Copy No.

47-48	Commanding Officer and Director Defense Technical Information Center Cameron Station, Building 5 5010 Duke Street Alexandria, VA 22314
	Science Applications International Corporation 1710 Goodridge Drive McLean, VA 22101
49	Attn: J. Hanna
50	R. Cavanagh
51	W. Monet
52	W. Renner
	Bell Telephone Laboratories, Inc. P.O. Box 496 Whippany, NJ 07981-0903
53	Attn: M. Pennotti
54	C. DeHaven
55	J. Eickmeyer
56	R. Patton
	Planning Systems, Inc. 7900 Westpark Drive, Suite 507 McLean, VA 22101
57	Attn: D. Pickett
	TRW, Inc. TRW Defense and Space Systems Group Washington Operations 7600 Colshire Drive McLean, VA 22101
58	Attn: R. Brown
59	R. O'Rear
	Bolt, Beranek, and Newman 1300 North 17th Street Arlington, VA 22209
60	Attn: M. Flicker
	ORINCON 1755 Jefferson Davis Highway Arlington, VA 22202
61	Attn: H. Cox

Distribution list for ARL-TR-90-37 under Contract N00024-86-C-6134, Task 1, Project 10 and Contract N00039-88-C-0043, TD Nos. 01A002 and 01A003 (cont'd)

Copy No.

General Electric Corporation
P.O. Box 4840
Syracuse, NY 13221-4840
62 Attn: J. Carlson

The Mitre Corporation
7525 Colshire Drive
McLean, VA 22102
63 Attn: K. Hawker

Woods Hole Oceanographic Institution
86-95 Water Street
Woods Hole, MA 02543
64 Attn: J. Lynch

Applied Research Laboratory
The Pennsylvania State University
P.O. Box 30
State College, PA 16801
65 Attn: S. McDaniel
66 D. McCammon

Marine Physical Laboratory
Scripps Institution of Oceanography
The University of California, San Diego
San Diego, CA 92132
67 Attn: F. Fisher
68 V. Anderson
69 W. Hodgkiss

Scripps Institution of Oceanography
The University of California, San Diego
La Jolla, CA 92037
70 Attn: Library

Director
North Atlantic Treaty Organization
SACLANT ASW Research Centre
APO New York 09019
71 Attn: Library
72 F. Jensen
73 T. Akal

Distribution list for ARL-TR-90-37 under Contract N00024-86-C-6134, Task 1, Project 10 and Contract N00039-88-C-0043, TD Nos. 01A002 and 01A003 (cont'd)

Copy No.

Defence Research Establishment Pacific
FMO Victoria, BC
VOS 1B0 CANADA
74 Attn: R. Chapman

Defence Research Establishment Atlantic
9 Grove Street
P.O. Box 1012
Dartmouth, NS
CANADA
75 Attn: D. Chapman

Applied Physics Laboratory
The Johns Hopkins University
Johns Hopkins Road
Laurel, MD 20810
76 Attn: J. Lombardo
77 A. Boyles

Department of Ocean Engineering
Massachusetts Institute of Technology
Cambridge, MA 02139
78 Attn: I. Dyer
79 A. Baggeroer

The University of Miami
10 Rickenbacker Causeway
Miami, FL 33149
80 Attn: F. Tappert

81 I. Tolstoy
Knockvennie, Castle Douglas
S.W. SCOTLAND
GREAT BRITAIN

Department of Geology
The University of Texas at Austin
Austin, TX 78712
82 Attn: C. Wilson

Distribution list for ARL-TR-90-37 under Contract N00024-86-C-6134, Task 1, Project 10 and Contract N00039-88-C-0043, TD Nos. 01A002 and 01A003 (cont'd)

Copy No.

Department of Physics
The University of Auckland
Private Bag, Auckland
NEW ZEALAND

83 Attn: A. C. Kibblewhite
84 C. T. Tindle

Department of Oceanography
Texas A&M University
College Station, TX 77843

85 Attn: A. Anderson

86 Environmental Sciences Group, ARL:UT

87 Nancy R. Bedford, ARL:UT

88 Karl C. Focke, ARL:UT

89 David E. Grant, ARL:UT

90 Robert A. Koch, ARL:UT

91 Stephen K. Mitchell, ARL:UT

92 Clark S. Penrod, ARL:UT

93 Jack A. Shooter, ARL:UT

94 Evan K. Westwood, ARL:UT

95 Library, ARL:UT

96 Reserve, ARL:UT